

Haptic-enabled Collaborative Virtual
Environments for Skills Training

HAPTIC-ENABLED COLLABORATIVE VIRTUAL
ENVIRONMENTS FOR SKILLS TRAINING

BY

SABA MOGHIMI, B.Sc.

A THESIS

SUBMITTED TO THE DEPARTMENT OF ELECTRICAL & COMPUTER ENGINEERING

AND THE SCHOOL OF GRADUATE STUDIES

OF MCMASTER UNIVERSITY

IN PARTIAL FULFILMENT OF THE REQUIREMENTS

FOR THE DEGREE OF

MASTER OF APPLIED SCIENCE

© Copyright by Saba Moghimi, June 2008

All Rights Reserved

Master of Applied Science (2008)
(Electrical & Computer Engineering)

McMaster University
Hamilton, Ontario, Canada

TITLE: Haptic-enabled Collaborative Virtual Environments
for Skills Training

AUTHOR: Saba Moghimi
B.Sc., (Electrical Engineering)
University of Tehran, Tehran, Iran

SUPERVISOR: Dr. Shahin Sirouspour

NUMBER OF PAGES: xiii, 86

To Shahin, my family, Fereshteh, and Amin

Abstract

Many manual tasks such as those in surgical applications require a high degree of motor skills that can only be gained through extensive training. This thesis is concerned with the design and control of collaborative training virtual environments with haptic feedback for skills training. The term "collaborative training" refers to a scheme in which the trainee and the trainer operate in a shared virtual environment. They collaboratively carry out the intended tasks using a shared "virtual tool". In order to enhance the trainee's motor skills, the conventional visual feedback will be augmented by force feedback providing the feel of the task environment as well as active guidance by the expert trainer.

First, a set of psychophysics experiments are designed to investigate the usefulness of haptic-enabled collaborative virtual environments for motor skills training. Eighteen volunteers randomly divided between two training and control groups have participated in the experiments. The training group would undergo a number of collaborative training sessions with active help from the trainer whereas the control group would try the task on their own to achieve a set of stated goals. Each of the experiments is designed with specific performance objectives in mind, including trajectory tracking and task completion time. The results of the psychophysics experiments confirm that, when visual feedback is partially impaired,

haptic-enabled collaborative training improves learning of a trajectory tracking task. In all the experimental scenarios tested, the results showed improvements in temporal response after receiving training.

The second part of the thesis is devoted to the development of a general control framework for the coordination of the users in haptic-enabled collaborative virtual environments. The haptic interface control design is separated from the virtual environment simulation in order to provide more versatility in control strategies for both impedance and admittance-type virtual environments. Adaptive nonlinear controllers are proposed that establish desired linear-time-invariant and/or nonlinear static mappings amongst the users and the virtual task environment positions and forces. These controllers account for the nonlinear model of haptic devices and can handle uncertainties in the haptic devices, the users, and the virtual environment dynamics. First, the tracking behavior of the system is shown via a Lyapunov analysis. Then using a priori known bounds on user and environment parameters, the robust stability of the system is analyzed by employing the Nyquist envelopes of interval plants and an off-axis circle criterion. The robust stability analysis provides bounds on the parameter of the linear and nonlinear mappings within which the stability of the system is guaranteed, for all possible system parameters with their a priori given bounds. Experiments carried out with two similar Quanser twin-pantograph haptic devices confirm the effectiveness of the proposed controllers in achieving the performance and stability objectives.

Acknowledgements

My thanks and appreciation to my supervisor, Dr. Shahin Sirouspour, for his guidance and kind support throughout my graduate program.

Sincere gratitude to my fellow colleagues in the Haptics, Telerobotics and Computational Vision Lab, Amin Abdossalami, Bassma Ghali, Behzad Mahdavikhah, Ali Shahdi, Sina Niakosari, Ramin Mafi, Bahram Marami, Pawel Malysz, Mike Kinsner, Peter Kuchnio, Ivy Zhong, Insu Park, Anthony Brown and all my other friends here at McMaster for being part of this wonderful journey.

Special thanks to Fereshteh for her support patience and motherly love, to Sahar and Behzad for their kind encouragement, and to my dear parents without whom none of this would be possible.

Contents

Abstract	iv
Acknowledgements	vi
1 Introduction	1
1.1 Motivation	1
1.2 Problem Statement and Thesis Contributions	4
1.2.1 Human Factor Studies	5
1.2.2 A General Control Framework for Human-haptic Guidance .	6
1.3 Organization of the Thesis	8
1.4 Related Publications	9
2 Literature Review	10
2.1 Haptic Simulation System	11
2.1.1 Human Operator	11
2.1.2 Haptic Interface	12
2.1.3 Haptic Control System	13
2.1.4 Virtual Reality Simulator	15
2.2 Stability and Control	16

2.2.1	Single-user Haptic Control Systems	17
2.2.2	Multi-user Systems	18
2.3	Applications	19
2.4	Psychophysical Evaluation of Haptic Guidance	21
3	Human Factor Studies	23
3.1	Psychophysical Experiments	24
3.1.1	Tumor Removal	25
3.1.2	Dimension Reduction in the Display	27
3.1.3	Combination of a Curvy Path and Dimension Reduction	28
3.1.4	Three Dimensional Curvy Path	29
3.2	Experimental Setup	32
3.3	Results	33
3.3.1	Discussion	35
4	Adaptive Controllers	42
4.1	System Dynamics	43
4.2	Control Design	45
4.2.1	Impedance-type Virtual Environments	47
4.2.2	Admittance-type Virtual Environments	48
4.2.3	Performance analysis	50
5	Robust Control Analysis	54
5.1	Linear Mapping	55
5.1.1	Case 1: $\frac{H_{fhe}}{H_{fhi}}$	59
5.1.2	Case 2: $\frac{H_{fh1}}{H_{fh2}}$	61

5.2	Nonlinear Mapping	61
6	Experimental results	68
6.1	Experimental Setup	69
6.2	Impedance-type Environment	70
6.3	Admittance-type Environment	71
7	Conclusions and Future Work	76

List of Figures

1.1	The concept of collaborative training in human-haptic guidance . . .	4
2.1	A generic block diagram representation of a haptic system and its components	11
2.2	Open-chain robotic manipulator by CRS Robotics	13
2.3	The Admittance-type haptic display known as Cobotic hand controller.(Picture from [1])	14
2.4	Examples of impedance-type haptic displays a) IHA developed by Quanser b) Phantom by SensAable c) 3 DOF Pantograph by Quanser d) Haptic Breadboard co-developed by McMaster and Quanser . . .	15
2.5	The impedance and admittance type virtual environment. X denotes the position and f is the force.	16
3.1	The virtual reality model displayed on trainee and trainer sides. 1. tumor removal grid-on, 2. tumor removal curvy path, 3. dimension reduction in the display, 4. combination of curvy path and dimension reduction.	37

3.2	A) Virtual reality display on the trainer side, B) Virtual reality display on the trainee side. The red ball marks the user position and the green balls represent three targets distributed on the purple sphere. The users were instructed to move from left to right.	38
3.3	The desired and the actual path presented to one of the users after the trial. (The balls mark the targets.)	39
3.4	The experimental set-up.	39
3.5	The mean error versus samples in the desired trajectory (The recorded desired trajectory consists of 273 samples. The first half of the path is marked with 1 and the second with 2).	40
3.6	Number of users versus different error ranges in meters.	41
4.1	Cooperative haptics control with impedance-type virtual environment.	48
4.2	Cooperative haptics control with admittance-type virtual environment.	49
4.3	Closed-loop system for impedance-type environments.	52
4.4	Closed-loop system for admittance-type environments.	53
5.1	Closed-loop system for impedance-type environments.	55
5.2	Closed-loop system for admittance-type environments.	56
5.3	Closed-loop system for impedance-type environments when all filters are LTI.	58
5.4	Closed-loop system for admittance-type environments when all filters are LTI.	59

5.5	Stability regions with respect to τ_1 and τ_2 : (a) Impedance-type environment in Case 1; (b) Admittance-type environment in Case 1; (c) Impedance-type environment in Case 2; (d) Admittance-type environment in Case 2.	60
5.6	Nonlinear Luré feedback form.	61
5.7	Closed-loop control system for interaction with a impedance-type environment transformed into nonlinear Luré form with $k_f(\cdot)$ as the nonlinear element. $u = f_h^{2*} H_{fh2} + f_h^{1*} H_{fh1} - \bar{\rho} + \frac{\rho_e(1-H_{x2})}{H'_{xm2}} (H_{zt} + H_{fh2}z_{h2})$	64
5.8	Closed-loop control system for interaction with an admittance-type environment transformed into nonlinear Luré form with $k_f(\cdot)$ as the nonlinear element. $u = \frac{f_h^1 H_{fh1} + f_h^2 H_{fh2}}{(\frac{H_{fh1}z_{h1}}{k_p H'_{xm1}} + \frac{H_{fh2}z_{h2}}{H'_{xm2}} + H_{zt})Y_e}$	64
5.9	Closed-loop control system for interaction with an impedance-type environment transformed into nonlinear Luré form with $k_p(\cdot)$ as the nonlinear element. $u = \frac{1}{H_{fh1}z_{h1} + H_{x1}z_e} (f_h^{2*} H_{fh2} + f_h^{1*} H_{fh1} - \bar{\rho} + \frac{\rho_e}{H'_{xm1}} (H_{x1}z_e + H_{fh1}z_{h1}))$	65
5.10	Closed-loop control system for interaction with an admittance-type environment transformed into nonlinear Luré form with $k_p(\cdot)$ as the nonlinear element. $u = \frac{f_h^1}{z_{h1}} + \frac{f_h^2 H_{fh2}}{z_{h1} H_{fh1}}$	66
5.11	The result of stability analysis for impedance-type for various tool damping values with nonlinear mapping sectors.	67
5.12	The result of stability analysis for admittance-type for various tool damping values with nonlinear mapping sectors.	67
6.1	Experimental Setup	70

6.2	Impedance-type with linear filters (a)Positions. (b) Estimated pa- rameters. (c) $H_{fh1}F_h^1 + H_{fh2}F_h^2, H_{fe}F_e, H_{fh1}F_h^1$, and $H_{fh2}F_h^2$	72
6.3	Impedance-type with a nonlinear mapping as k_f (a) Positions. (b)Estimated Parameters. (c) $H_{fh1}F_h^1 + H_{fh2}F_h^2, H_{fe}F_e, H_{fh1}F_h^1$, and $H_{fh2}F_h^2$	73
6.4	Admittance-type with linear filters (a)Positions. (b)Estimated pa- rameters. (c) $H_{fh1}F_h^1 + H_{fh2}F_h^2, H_{zt}x_e, H_{fh1}F_h^1$, and $H_{fh2}F_h^2$	74
6.5	Admittance-type with a nonlinear mapping as k_f (a)Positions. (b) Estimated parameters. (c) $H_{fh1}F_h^1 + H_{fh2}F_h^2, H_{zt}x_e, H_{fh1}F_h^1$, and $H_{fh2}F_h^2$. 75	

Chapter 1

Introduction

1.1 Motivation

Human operators are always seeking to gain dexterity in different manual skills. These motor skills can range from developing fine surgical skills to learning sports techniques. Therefore, the development of effective motor skills training methods seems crucial. One of the training methods recently introduced is using virtual reality simulation. Virtual reality simulation is an engine that enables interactions with a computer-simulated virtual environment. A good example is the use of virtual reality simulation for surgery training. The conventional surgery training method consists of attending a number of surgery sessions. Nowadays, using virtual reality simulators for surgery training is an effective way for students to master the surgical procedure virtually before actual trials on patients [2,3]. Using virtual reality simulators for training has many advantages over the conventional methods. Working on a virtual model helps avoid the risks and costs associated

with performing the actual task. This approach is more flexible in terms of adjusting the difficulty of the task and providing extra information and guidance. Moreover, different aspects of the trainee's behavior such as the temporal response as well as trajectory and force profiles in completing the task can be recorded during the training. These recorded data enable detailed analysis of the human user performance as they try different scenarios, and then you can use this data to find the correlation among the task parameters and learning and perhaps to adjust the training scenario accordingly.

In early virtual reality simulators, the human user was provided by a visual display of the virtual environment through the computer screen or stereoscopic display. These simulators enabled navigation in the virtual world, but the ability to feel the virtual object was missing. Haptic displays were later introduced to increase the realism in interactions with the virtual objects [4,5]. With the aid of haptic displays the human operator is able to feel the virtual environment through kinesthetic and force feedback provided. A haptic system consists of a robotic interface and a control and simulation engine to provide realistic interactions between the human operator and the virtual environment.

Haptics has been widely used for enhancing realism in virtual reality applications. If used in conjunction with an appropriate simulator representing the intended task, haptic interfaces can be a powerful training tool. Force feedback provided through haptic interfaces can be used to augment the existing audio-visual based training techniques and potentially increase their effectiveness. Haptic-enabled virtual reality simulators can be used for displaying pre-recorded trajectories, introducing virtual barriers [6] or providing the means to model real world

skills training tasks [2].

Haptic-guidance using pre-recorded or computer generated data for training has been studied before in the literature. However, replacing the training data sets with an active intervention from an expert trainer may be more effective for teaching motor skills for certain applications. This new paradigm will be referred to as human-haptic guidance. In this thesis, the trainer can actively intervene and guide the trainee throughout the simulated task.

While guidance may also be provided through active replay (i.e. using a haptic display) of the task, interactive participation of the trainer in human-haptic guidance systems provides greater flexibility in correcting the trainees errors in real-time particularly in complex procedures. Using human-haptic guidance, novel training techniques can be developed to allow surgeons to interactively work with a trainee in a simulated surgery platform teaching fine manipulation skills. Using this training method can also improve the ergonomics of training by enabling the trainee and the trainer to participate in the task from separate workstations. Haptic-based tele-rehabilitation can improve the existing post-injury recovery techniques. A therapist can remotely guide the patients in performing physical exercises in a virtual environment and, therefore, obviate patient transportation and facilitate the recovery process. There is need for evaluating the effectiveness of this training paradigm in developing human motor skills. Moreover importantly, new control methods must be developed for stable interaction of the users in human-haptic guidance systems.

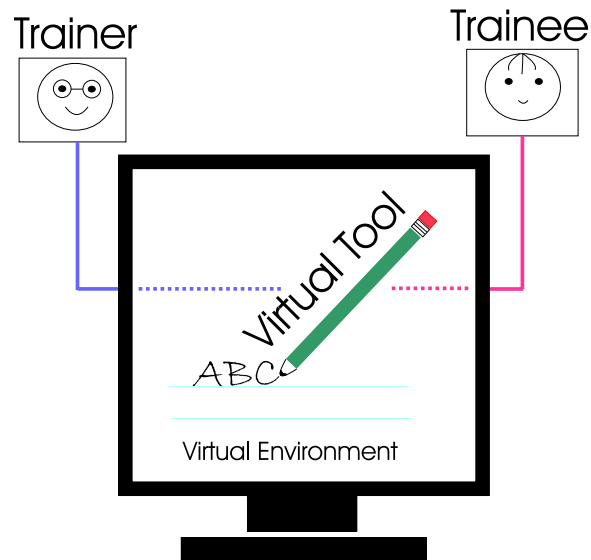


Figure 1.1: The concept of collaborative training in human-haptic guidance

1.2 Problem Statement and Thesis Contributions

Figure 1.1 depicts a general overview of a human-haptic guidance system also known as collaborative training method. Collaborative training involves linking the trainer, trainee, and the virtual environment through a virtual tool. In this framework, the users would feel each other's motion and force as well as the response to their action in the form of the environment force. This training concept can be interpreted as a scenario in which the trainer is holding the trainee's hand guiding her through the process. In other words, the users cooperatively manipulate a virtual tool through which they come in contact with the environment and feel its reaction force. Note that each of the users has her own haptic device and the link is created through the control system.

This thesis is concerned with assessing the usefulness of collaborative haptic

training and developing a general control framework enforcing this training platform for stable interaction in human-haptic guidance systems. The contributions of the thesis are summarized below.

1.2.1 Human Factor Studies

A series of psychophysics experiments are designed and conducted to test the ability of collaborative haptic training method in motor skills learning. Different experimental scenarios are attempted and an optimal experimental design is proposed. Eighteen subjects are randomly distributed in two groups. Subjects in the first group known as the control group try the experiment scenario on their own, whereas the second group members can choose between receiving collaborative haptic training and trying the task themselves. The performance of the two groups is compared with each other to capture the effectiveness of collaborative haptic training. The parameters evaluating the performance include the time spent to complete the task and the error in tracking the 3D trajectory introduced in the experimental scenario.

In all of the experimental scenarios attempted, receiving the training reduces the task completion time. However, it is in the latest experimental scenario that the trajectory tracking accuracy noticeably improves. In these final experiments the subjects are required to follow a 3D trajectory on the surface of a sphere. The virtual sphere is displayed on a two-dimensional computer screen. In this scenario the lack of the depth perception forces the subjects to follow the trainer attentively as she guides them along the path. As a result, an obvious improvement is detected in the trajectory tracking error for the training group.

The results of the human factor studies show the effectiveness of the collaborative haptic training in the proposed experimental scenarios. These results motivate the development of a general control framework for human haptic guidance that provides greater flexibility in how the trainer, trainee and the virtual environment are linked to each other.

1.2.2 A General Control Framework for Human-haptic Guidance

The control objectives need to be defined to enable the desired link between the trainee, the trainer and the virtual environment. The performance of the control system in achieving the objective has to be assessed. Later, the stability of the closed-loop system needs to be evaluated.

- **Performance**

In order to create a link between trainee, trainer and the environment, both force and position should be taken into account. The development of simulators for training purposes may also involve different mappings. In many applications the users are interested in magnifying the workspace for more accuracy. In systems involving more than one user controlling the same object, an authority sharing between the users is necessary to define their relative dominance in the control. A general formulation of the desired control objectives for force and position tracking allowing desired mappings is presented in (1.1) and (1.2) respectively.

$$\alpha_{f1}f_{h1} + \alpha_{f2}f_{h2} = z_t x_t + k_f(\alpha_{fe}f_e) \quad (1.1)$$

$$\alpha_{x1}k_p(x_1) = \alpha_{x2}x_2 = \alpha_{xt}x_t \quad (1.2)$$

Here f_{hi} is the hand force of the i^{th} user, z_t is the impedance of the tool, and α is an LTI filter applied to the element specified with the indices; k_p and k_f represent static nonlinear monotonic position and force mappings accordingly. As for the indices, $i = 1$ represents the trainer, $i = 2$ the trainee, and e the virtual environment.

Satisfying the criteria presented ensures the connection of the operators through a virtual tool with the mechanical impedance given by z_t . In the most simple case where k_f and k_p are linear coefficients and $\alpha_{f1} = \alpha_{f2} = \alpha_{fe} = \alpha_{x1} = \alpha_{x2} = \alpha_{xt} = 1, k_f = k_p = 1$ the force and position transparency objectives transform into

$$f_{h1} + f_{h2} - f_e = z_t x_t \quad (1.3)$$

$$x_1 = x_2 = x_t \quad (1.4)$$

According to (1.3) the net force is applied to the virtual tool with its dynamics represented as z_t . In this case the trainee and the trainer are perfectly following each other according to (1.4), and the virtual tool position is set to be the same as the position of the human operators.

The controller should be designed for each of impedance and admittance-type virtual environments which will be introduced in the next chapter.

An adaptive controller is proposed to compensate for the uncertain nonlinear dynamics of the devices and the users. Using a Lyapunov analysis, it is shown that the proposed adaptive control framework can establish the desired mappings in the presence of nonlinear dynamics of the haptic devices, and structured parametric uncertainty in the users, environment and device dynamics.

- **Robust Stability**

The Lyapunov stability analysis ensures the performance of the system in achieving the desired transparency objectives. However, the closed-loop stability of the system has to be investigated for different filter parameters. In the presence of uncertainties in the form of user and environment parameters. It should be noted that these parameter uncertainties are assumed to be bounded by known values.

The regions of robust stability are investigated for different mapping parameters. The algorithm proposed in [7,8] is modified for collaborative handling of the virtual tool. Different mappings are included and closed-loop stability in the presence of uncertainties is analyzed using the Nyquist envelop of interval plants and an off-axis circle criterion.

1.3 Organization of the Thesis

The rest of this thesis is organized as follows. Relevant literature addressing haptic interfaces, applications and previous human factor studies in this field is presented in Chapter 2. In Chapter 3 the effectiveness of the proposed collaborative training

framework is tested in a series of psychophysical experiments. The adaptive controllers that enforces the the collaborative training regime and the force and position tracking objectives are introduced in Chapter 4. The robust stability analysis of the closed-loop system for linear time invariant (LTI) filters and static nonlinear position and force mappings in the presence of user and environment uncertainties is analyzed in Chapter 5. The experiments conducted to evaluate the performance of the proposed controllers are presented in Chapter 6. The thesis is concluded in Chapter 7 where some possibilities for future work are also discussed.

1.4 Related Publications

- S. Moghimi, S. Sirouspour, and P. Malysz, "Haptic-enabled Collaborative Training with Generalized Force and Position Mappings," Symposium on Haptic Interfaces for Virtual Environment and Teleoperator Systems, March 2008, Reno, NV, pp. 287-294.

Chapter 2

Literature Review

This chapter focuses on reviewing the previous studies in haptics systems and its applications. A general overview of a haptic system followed by the description of each of its components is presented. Stability of haptic control systems has been subject of extensive research and therefore, is also included in this review. Applications of haptics in different areas including in gaming, skills training and telerehabilitation are discussed. Finally, previous human factor studies concerning the haptic-guidance systems for skills training are reviewed.

2.1 Haptic Simulation System

A general representation of a haptic display system is illustrated in Fig. 2.1 where a human operator interacts with a virtual reality simulator and can receive kinesthetic and force feedback from virtual objects. A brief description of the components of the haptic simulation system follows next.

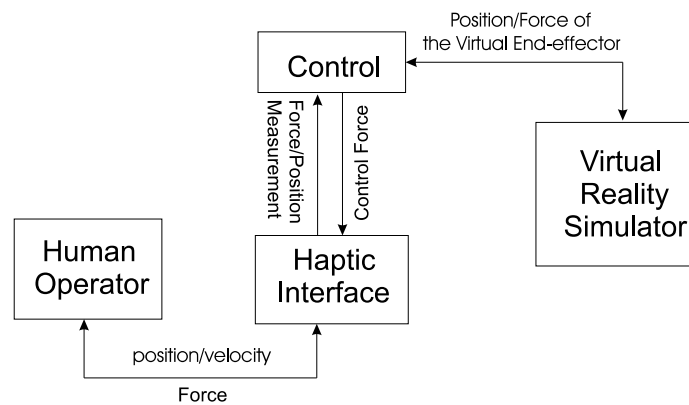


Figure 2.1: A generic block diagram representation of a haptic system and its components

2.1.1 Human Operator

The operator is always part of the system and has to be incorporated in any performance and stability analysis. Many studies have modeled the operator with a second-order linear time invariant model(LTI) (see [8,9]). In such approaches, the user arm is modeled by a passive mass-spring-damper mechanical impedance in series with a bounded exogenous force representing the user intentional force. The user moves the haptic device and feels the force feedback resulted from interacting with the virtual environment.

2.1.2 Haptic Interface

The haptic interface is composed of a mechanical device and other hardware components such as sensors for measuring the user position and/or force, and actuators that would apply the calculated environment reaction force to the user. There are many haptic devices currently available including joysticks, gloves [10], magnetically levitated wrists [11], and motion platforms with haptic display [12]. A large class of haptic interfaces in this thesis are robotic manipulators which provide kinesthetic and force feedback and in some cases tactile feedback to the user.

Robotic manipulators can be actuated in an open-chain kinematics structure where there is only one sequence of joints and links (arms) connecting the base of the manipulator to the end-effector (see Fig. 2.2). Another actuation mechanism is based on a closed-chain structure in which a number of the links form a loop as in the 3 DOF Pantograph by Quanser Fig. 2.4.b. The first structure usually provides a larger workspace and has a less complicated direct kinematics calculation whereas the second can yield a larger force output with relatively easier inverse kinematics calculations.

Haptic devices can also be classified into impedance and admittance-types. The admittance-type devices are usually controlled by admittance-type controllers and have large inertia and high output forces. These haptic displays are highly geared and therefore are non-backdrivable [13]. Hapticmaster [14] and the Cobot Hand Controller [13] Fig. 2.3 are examples of this category of haptic devices. The admittance-type devices are often costly and are best suited for displaying rigid constraints [13].

Examples of another haptic device category known as impedance-type haptic



Figure 2.2: Open-chain robotic manipulator by CRS Robotics

devices are depicted in Fig. 2.4. Impedance-type device are suitable for simulations of low-inertia virtual environments. Various types of these devices have been developed and are commercially available including Phantom (SensAble) Fig. 2.4.a and the Twin Pantograph (Quanser, Markham, Ontario) Fig. 2.4.b. Impedance-type haptic devices have low-inertia and high back-drivability, and are controlled by impedance-type controllers. They perform the best in free motion and in contact with soft environments.

2.1.3 Haptic Control System

The control system has to maintain a stable interaction between the haptic interface and the virtual environment. The controller requires measurements in the form of

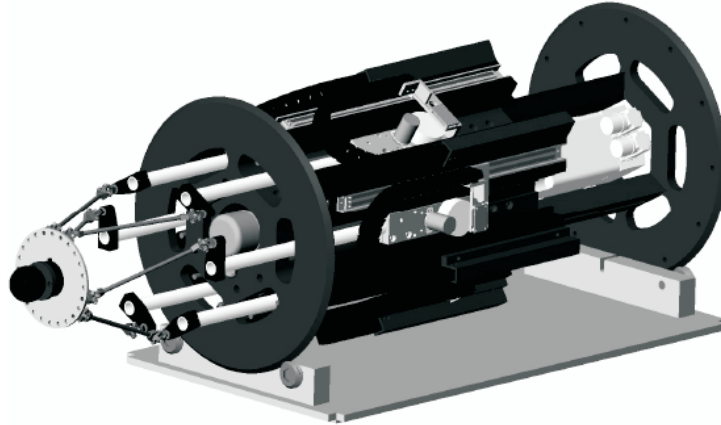


Figure 2.3: The Admittance-type haptic display known as Cobot hand controller.(Picture from [1])

force and/or position depending on the haptic device type. The controller should render a realistic feel from the virtual objects through kinesthetic and force feedback. There are two essential objectives in control design known as transparency and stability. The transparency is a measure of the fidelity of the virtual environment. In an ideal transparent haptic simulation the user should feel that she is directly interacting with the objects in the environment [15]. Therefore, to optimize the transparency, the interfering effect of the device dynamics has to be minimized and highly rigid contacts must be stably rendered. The stability is concerned with preventing unwanted oscillations which can degrade the performance of the system, damage the system and cause harm to the user. A more detailed discussion of different control strategies attempted in the literature will follow shortly.

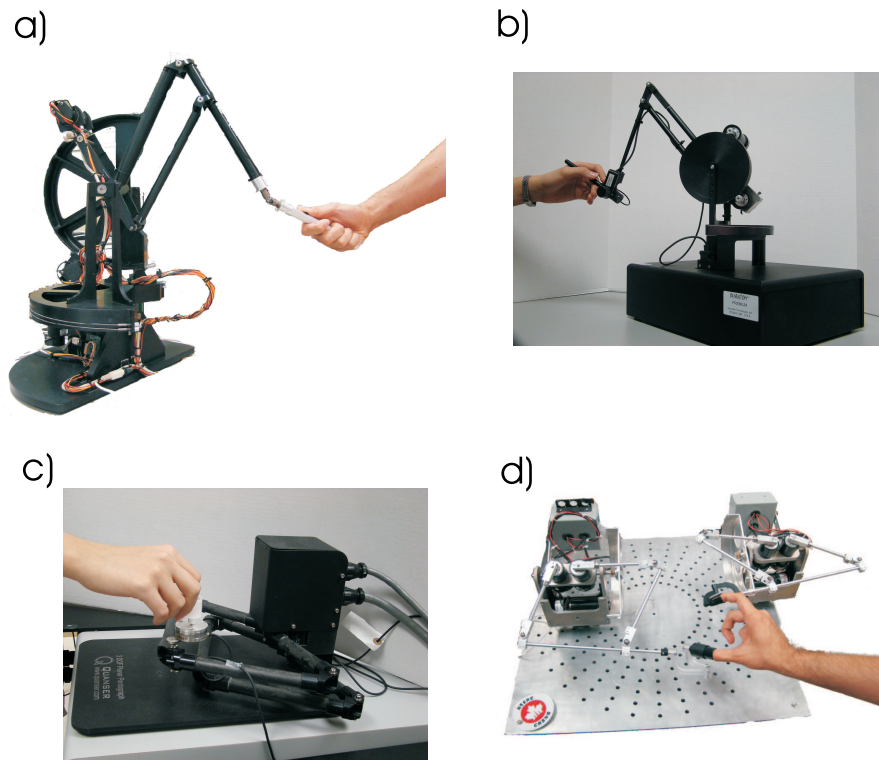


Figure 2.4: Examples of impedance-type haptic displays a) IHA developed by Quanser b) Phantom by SensAble c) 3 DOF Pantograph by Quanser d) Haptic Breadboard co-developed by McMaster and Quanser

2.1.4 Virtual Reality Simulator

The virtual reality simulator provides a visual display of the virtual environment for the human operator to explore, and usually incorporates dynamic simulations to calculate the motion and the forces resulting from the user interaction with the virtual objects. Based on the control algorithm and the haptic device type, the virtual environment can either respond to force or position of the user. An impedance-type environment generates interaction force based on the physical model and in response to the user motion. An admittance-type virtual environment calculates the motion of the haptic device based on the user input force [16].

(Generic illustrations of virtual environments simulators are given in Fig. 2.5.).

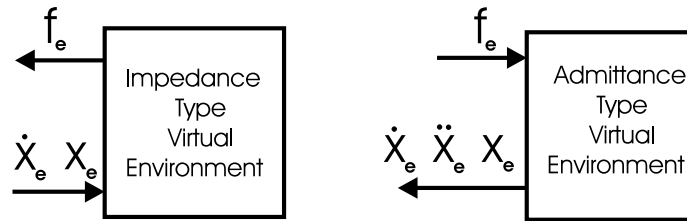


Figure 2.5: The impedance and admittance type virtual environment. X denotes the position and f is the force.

2.2 Stability and Control

A haptic system is consisted of both continuous and discrete-time components. The human operator and the haptic device are continuous-time elements of the system whereas the parts executing on the computer system including the controller and the environment simulator run in discrete-time. Optical encoders are often used to measure the position of haptic devices. The output of the optical encoders are quantized which may cause limit cycles, and can lead to instability of the system specially if its outputs are differentiated to access velocity [17]. Actuator dynamics and the fact that velocity is usually obtained from position measurement filtering are other possible sources of performance degradation and instability.

There has been a healthy body of research on analyzing the stability of the system in haptic interfaces. These studies are discussed throughout the rest of this section.

2.2.1 Single-user Haptic Control Systems

Research on single-user haptics leads to numerous rendering and control algorithms for force and kinesthetic feedback. In this framework, a single user comes in contact with a virtual environment through a haptic interface. A lot of studies in this field are focused on providing a reliable and stable connection between the human operator and the virtual reality.

Different studies in the literature have used passivity as a means of ensuring stability, and found different conditions for the passivity of the system [16–21]. A system is known to be passive if the energy provided to the user is less than or equal to the energy supplied by the user to the system. It should be noted that passivity is only a sufficient condition for stability which could be overly conservative.

Colgate et. al [17] discussed that one important factor for evaluating the performance of the haptic interface is the Z-Width. The Z-Width is the range of the impedance that can be stably achieved. Using passivity analysis of a haptic interface, the authors found a lower bound for the feasible damping of a virtual spring-damper wall required for maintaining stability. This lower bound depended on the physical damping of the system, the sampling rate, and the stiffness of the virtual wall. Adams and Hannaford [16] investigated the stability and tried to maximize the performance of the haptic system at the same time. using a two-port model for both impedance and admittance type environments, they found that the physical damping and the conductance of the virtual spring-damper wall had to be non-zero and positive. They also discovered that for the impedance-type virtual environment, increasing the damping of the device, increased the maximum impedance that could be achieved.

Different studies were conducted to add physical dissipation to the system for improving stability. In [22] the use of inherent resistor-inductor of the motor in a voltage drive analog circuit was proposed to increase the maximum achievable stiffness. In [23], the authors proposed adding a programmable viscous damper using a time-domain passivity control methodology.

Abdossalami and Sirouspour [24] proposed novel adaptive control techniques for stable interaction with impedance and admittance-type virtual environments. The adaptation routine replaced the dynamics of the haptic interface that of an adjustable mass-damper. The method used both force and position measurements and proved to be highly effective in achieving stability for virtual environments with much higher stiffness than previous studies.

2.2.2 Multi-user Systems

In many haptic applications such as network-based gaming, training, and tele-rehabilitation it is required for multiple users to work cooperatively. Another application is in teleoperation (control of a slave robot remotely by moving a master haptic device) where cooperative handling of the task might be necessary. Nudehi et. al [25] introduced a shared control approach to haptic interfaces for training purposes in minimal invasive surgery over long distances. In their approach, the surgeon and the trainee collaboratively controlled a surgical robot. Using H_∞ robust control stability analysis [26] and dynamic compensation, they created a shared control regime, and found conditions for ensuring stability.

Sirouspour [27] proposed an architecture for multiple users (masters) controlling multiple robots (slaves) cooperatively using robust control analysis. Other

studies of multi-master multi-slave architectures include [28] where adaptive control was used for dynamic compensation.

Multiple users can also be working cooperatively in virtual environments. There has been several studies on network-based cooperative handling of virtual environments. In [29], the authors proposed the use of state prediction to compensate for the negative effects of the network delay. An optimization problem was formulated to calculate the control gains to improve the performance while maintaining the stability. In [30] the use of a multi-rate control strategy was proposed in which the local feedback loop was executed at a higher rate than the data packet transmission enabling high-fidelity haptic rendering.

Khademian and Hashtrudi-Zaad [31] proposed a collaborative haptic training algorithm where the instructor and the trainee would try to complete a task in the virtual environment while interacting with each other. To analyze the stability issues in their design, the authors followed their work with a robust shared control analysis in [32].

2.3 Applications

Haptics has a wide range of applications for entertainment purposes. In many modern computer games, the consoles can provide the users with kinesthetic and force feedback. Some of the most common examples of rudimentary haptic feedback are the steering wheels providing a sense of the road as the player accelerates and maneuvers around in the race, Sony's Dualshock and the Nintendo Wii.

Training in virtual environment can be used for teaching skills in various fields of science. Once the intended workspace is modeled in virtual reality, the users can

test various scenarios which may be risky or costly if tried in real world. One of the fields in which haptic training has been used is in non-invasive surgery where avoiding all risks to the patients is vital. Kuhnappel et. al [2] developed a haptic interface system called *HapticIO* for Minimally-Invasive Surgery (MIS) training in virtual reality. Webster et. al [3] designed a haptic suturing simulator for wound closure where soft tissue modeling and recording of the user motion for later analysis was provided. Gunn et. al [33, 34] developed a surgical training method which allowed interaction between the experts and the trainee in the virtual environment. The users received kinesthetic and force feedback from the organ which they could also observe on a screen.

Jung Kim et. al [35] performed a study of collaborative haptics interactions over large distances. They conducted the experiments between the Touch Lab at MIT, USA and Virtual Environments and Computer Graphics lab at University College London, UK. The authors used questioners for evaluating the performance of the system and found that the copresence of the users was improved when kinesthetic feedback was provided.

Haptic-guidance has also been used for calligraphy teaching. Henmi et. al [36] used haptic training for calligraphy lessons in Japanese. A record and replay of the expert hand motion was used in this study. Yokokohji et. al [37] focused on developing a visual/haptic training system to improve hand-eye coordination. They investigated the sliding of a virtual cube on a rigid table as a benchmark for skills training. The display was called WYSIWYF (What You See Is What You Feel). Recording and replaying the teacher's hand motion was used in their approach.

Carignan and Olsson [38] proposed the use of haptic guidance for rehabilitation over the internet. Their scheme enabled patients to participate in therapy sessions remotely which made the rehabilitation process much more accessible and convenient for them.

2.4 Psychophysical Evaluation of Haptic Guidance

To evaluate the effectiveness of haptic guidance in teaching skills, different psychophysical experiments have been performed, and have resulted in interesting findings. A comprehensive review of the experiments conducted evaluating the use of robotics for skills training can be found in [39]. In this review different methods have been discussed in which the task dynamics were altered to improve conventional training.

Feygin et al. conducted a series of human factor studies comparing performance in experiments providing sheer haptic, visual or combined haptic and visual feedback to different test groups [40]. A 3D desired trajectory was generated by combining sine waves fluctuating along different position axes with various frequencies. In this study the subjects with visual feedback could observe the haptic device as it moved along the desired trajectory, and virtual environment display was not provided. The use of a combined version of haptic and visual displays was eventually concluded to perform the best.

Liu et al. performed a set of human factor studies for rehabilitation purposes [41]. Taking up a similar approach as that in [40] with less complicated desired trajectories, they concluded that vision alone would perform slightly better than the combined visual and haptic training.

Other relevant studies include evaluation of force pattern [42] and calligraphy training [35] which both confirmed the effectiveness of the use of haptics in teaching motor skills.

Chapter 3

Human Factor Studies

A series of human factor studies are conducted to evaluate the effectiveness of human-haptic guidance in skills training. In order to assess the ability of the collaborative training to teach the intended task, the subjects are randomly distributed in two groups, namely training and control. Members of the training group receive haptic-guided training whereas the subjects in the control group try the task on their own only using visual feedback. Various experimental scenarios are attempted to compare the performance of these two subject groups which will be discussed throughout this chapter.

The first part of this chapter focuses on the design of the experiments. In the second part, the results and the methods used for comparing the performance of the subjects is discussed. Finally, a comparison between the two groups of subjects is performed, and other relevant findings are reported.

3.1 Psychophysical Experiments

In order to achieve the optimal experimental design for the psychophysical experiments capturing different features of an actual training session, different scenarios are tested. A brief description of each of these primitive training scenarios followed by the resulting final design is presented below.

The subjects are divided in two groups: the training and the control group. Subjects in the training group undergo a number of training sessions with active help from the trainer whereas those in the control group receive no active training in completing the assigned tasks. In an actual training session, the trainer should have a higher level of expertise due to her experience and understanding of the specific training task. However, our studies are to test the method in a general training situation focusing on specific aspects of learning. Therefore, the trainer and the trainee share the same level of acquaintance with the task. In order to ensure that the trainer will master the task, she is provided with artificial privileges such as virtual fixtures [43] and more details in the virtual environment display. This will be discussed in details later in the following sections.

Two separate displays of the virtual environment are developed and are presented to the trainer and the trainee during training sessions. The subjects are advised to follow the motion on the monitor, but their view over the haptic device is unobstructed.

Throughout this chapter we are investigating the effect of collaborative haptic training in:

- Reducing the task completion time

- Reducing the error in the trajectory tracking task.

3.1.1 Tumor Removal

In this task, the trainee is asked to remove a set of four balls from a big encircled area. The workspace is chosen to be a two dimensional planar representation. Fig. 3.1.1 and 3.1.2 illustrate the virtual reality displayed to the trainer and the trainee. The task involves penetrating the big circle representing an organ, and reaching out for each of the four smaller circles representing tumors in a specific order. In order to penetrate the organ the user has to exceed a minimum threshold force, and to drag the tumors out she has to apply enough force for the ball to be attached to the tip of the device. Once the tumor is attached to the tool, the trainee can drag it out of the organ for it to disappear which signals her success. Two of the tumors are stationary whereas the remaining two are moving on a predefined path. The users are asked to follow a certain trajectory to get to the static tumors, whereas, for removing the tumors, they are instructed to minimize the time and the distance traveled inside the organ to reduce tissue damage.

To make the task more challenging on the trainee side, the motion of the trainee is implemented in a non-intuitive form. Such non-intuitive eye-hand coordination problems can be experienced during manipulation tasks such as Laparoscopic surgery. In this configuration, the trainee's hand motion will result in the movement of the tool tip in the reverse direction along x and y .

Trajectory Comparison:

To compare different trajectories the time index has to be removed and the recordings has to be resampled so all have the same dimensions. In order to get

the same number of samples for all users, the sampling is carried out based on the normalized length of the trajectory. The length of the traveled distance is first extracted by point to point integration. The new samples are then drawn with a step size $\Delta = \frac{D}{N}$ where N is the target number of samples and is the same for all users to make comparison feasible. The resampling process starts from the first element in the data set. The second sample will be on a line resulting from interpolation between the first point and the next point in the data set and is Δ step away from the previous resampled point. If the next point is represented by (x_e, y_e) and the previous resampled one by (x_o, y_o) , the desired point (x, y) needs to satisfy

$$(y - y_o)(x_e - x_o) = (x - x_o)(y_e - y_o) \quad (3.1)$$

$$\Delta^2 = (y - y_o)^2 + (x - x_o)^2$$

Following the same procedure for each user results in N samples of x and y . The difference between the original and resampled data is barely noticeable with a sufficiently large value for N .

Grid-on:

At this stage, the desired trajectory to grab the stationary tumors is in the form of squares marked in a two dimensional plane. A view over the virtual environment on both trainer and trainee side is provided in Fig. 3.1.1. The path is visible to the trainer, but the trainee will just see grids paving the workspace. The grid will help the trainee remember the approximate path.

The training group are guided through the aforementioned collaborative training algorithm during five trials, and the control group has sheer visual feedback

in five trials where they can observe the trainers path on their screen visually. In order to provide a fair set of experimental conditions, the subjects in the control group are allowed to try the task five times on their own. Without any help from the trainer, they will try to fulfil the task and remove the tumors as discussed.

No significant difference between the two groups is noticed in following the trajectories. This is due to the fact that the display grids provided in this set-up give an advantage to the subjects in the control group for they have the opportunity to visually memorize the path before the actual trials. Therefore, in a revised version of the experiment, the grids are removed and a curvy path is chosen to reduce the possibility of path memorization by the control group.

Curvy path:

During these trials the view over the workspace is provided to the trainee, but the viewpoint overlooking the scene is twisted by 45° with respect to the base frame of the target training area for the trainee. Fig. 3.1.2 depicts both trainee and trainer displays in one of the training sessions. The differences in the visual display provided to the users in order to provide artificial advantages to the trainer can be followed in this figure. In these experiments, the results from the training group do not reveal any major improvement in trajectory tracking. To make the task more challenging, the dimension of the display on the trainee side is reduced and the task scenario is modified in the next approach.

3.1.2 Dimension Reduction in the Display

In this configuration seven balls are distributed in a two dimensional plane as targets. The targets appear in blue and red, and based on the colors the users are

instructed to come in contact with the front or the back of the object. Following this procedure will eventually lead to moving in a certain path. The trainee's viewpoint, however, is in the same plane as the targets resulting in the loss of depth perception. This will render visual feedback insufficient in the training task. Therefore, the users are forced to use the force feedback guiding them to compensate for the lack of a perfect visual feedback. Fig. 3.1.3 depicts the environment displayed to each of the users.

The non-intuitive motion is deactivated at this stage to make it easier for the subjects to focus on the depth of the space. However, the users in both groups tend to ignore the motion economy, and deviate from the target path. The users also use motion in x direction to figure out if the target is to the front or the back of the current position of the tool. Although this technique helps both trained and non-trained subjects fulfill the task, it degrades their performance in following the trajectory. Since the trained users are also focused on using the visual feedback to find the right path they unintentionally ignore their haptic trainings. Therefore, no significant difference in the performance of the trained and non-trained users is observed in trajectory tracking accuracy.

To encourage the subjects to take trajectory tracking into consideration, the reduced dimension display is combined with motions on curvy paths between subsequent targets.

3.1.3 Combination of a Curvy Path and Dimension Reduction

The users are asked to move on a curve which is part of a circle as shown in Fig. 3.1.4. The number of the targets is reduced from seven to three to make it

easier for the subjects to remember the path and to focus on the quality of the task completion rather than the quantity of the remaining targets. The results of this experimental design fail to show any significant improvement in following the desired trajectory.

None of the experiments discussed so far reveal any noticeable difference between the two test groups. The 2D planar format of the experiments is believed to have degraded the results. Therefore, motion in a 3D space is considered. Nonetheless lessons learned from these experiments lead to the design of the final training scenario which later is proved to be successful in capturing the effect of haptic training.

3.1.4 Three Dimensional Curvy Path

Since the use of two dimensional trajectories failed to capture the effect of training for previously discussed reasons, a 3D dimensional virtual training task is considered instead. The new experiments are also using a curve as the desired trajectory. inspired by the work in [40] a new scheme is designed. Since the three dimensional workspace is presented on a two dimensional display, the user will not still have a perfect visual feedback and will be encouraged to pay attention to the trainings.

Based on the results of prior experiments, keeping the training group engaged in the experiments is found to be critical. People subject to sheer training are found to be disengaged and passive resulting in a degraded performance. Therefore, a mixed trial and training strategy is employed during which the subjects can choose if they want to receive a training session or try the task by themselves. The combined number of trials and trainings is limited to the same number of trials allowed

for the control group.

The effect of vision and haptic displays on improving trajectory tracking has been studied before in [40]. In this study, when providing visual feedback to the user, the subject has a complete view over the haptic device and the workspace. As a result, the visual feedback overshadows the unconventional training through haptics. In many tasks including endoscopic surgery the view over the workspace is provided through a 2D display. Presenting a 3D workspace through a 2D display provides a defective visual feedback lacking depth perception. In such applications, the lack of sufficient information in vision cues forces the the subjects to use other sensing modalities such as kinesthetic and force feedback. Haptic guidance can potentially play an important role in training of such tasks. This motivates the redesign of the training scenario to study tracking of a 3D trajectory displayed on a 2D display.

The desired 3D trajectory is consisted of two curves on the surface of a sphere connecting three target points located on the surface as well. The subjects are instructed to travel the minimum distance between target points which is essentially an arc formed by the intersection of a plane passing through the center of sphere and the target points, and the sphere, i.e. see Fig. 3.3. In order to provide the trainer with the ability to master the task, she is equipped with haptic feedback from the virtual sphere and the two intersecting planes representing the curves. This feature works as a virtual fixture [43] giving her the advantage to feel the surface of the sphere and the planes marking the trajectory. Moving along the intersection of the plane and the sphere, she can lead the motion of the trainee to the desired path. The trainer can also see the planes in her display. Fig. 3.2 is a screen shot of

the view of the trainer and the trainee from the virtual task. The deficient 2D presentation is the same for both training and control group. However, the subjects in the control group are provided with an off-line 3D display of the path traveled and the desired path. The subjects can explore these trajectories from different viewing angles upon request. Fig. 3.3 shows this off-line display of the trajectories for one of the subjects in the control group.

Procedure:

The test group consists of 18 healthy volunteers aged between 23 to 28, six of which were female. All the subjects are graduate students at MacMaster University. The trainer is a female student in charge of conducting the experiments. The best performance is promised to be compensated with a gift as a motivation.

Each subject can try the experiment ten consecutive times. The users in the training group can choose if they wanted to receive training or try the experiment on their own before starting each test. The total number of trial or training is limited to ten for both groups. The data is recorded immediately after the tenth trial where the users try the task on their own.

Data Analysis:

Finding the deviation from the 3D desired path requires development of a specific graphical analysis. The recorded data has different number of samples. The difference in the size and the speed of motion makes a direct sample by sample error calculation impossible. In order to develop an error measurement algorithm, a local search based on the graphical properties of the experiment is developed. The desired trajectory is first recorded from the trainer side after she moved the device along the target path. The path recorded consists of a certain number of

data samples. The goal is to find the error between each of these samples and the closest point recorded from the subject. As mentioned before, each segment of the path is the result of passing a plane X_i ($i = 1, 2$ for the first and second segment respectively) from the center of the sphere and the two targets specifying the beginning and the end of this segment. To find the error at each sample for the i^{th} segment, a plane Y is formed passing through that sample point and the center of the sphere and is chosen to be perpendicular to plane X_i . Then, the recorded data is searched to find a point a with minimum distance from the plane Y . The error at the previously chosen sample point of the desired trajectory can then be found by calculating the distance between point a and the sample point under investigation.

Since the aforementioned method of finding the error may be rewarding to users who choose to have a fidgety motion around the desired path, the length of the path the user traveled is also calculated using integration. This length is compared to the length of the desired trajectory to avoid encouraging long paths and unnecessary loops along the way.

3.2 Experimental Setup

The experimental set-up used in this paper is shown in Fig. 3.4. On the trainer side a 6DOF Phantom device from Sensable, and for the trainee a 3DOF IHA haptic interface by Quanser is used. The IHA robot can apply forces up to 100 N, and is suitable for providing the desired authority sharing without going to saturation as a result of large forces possibly applied to oppose the trainee's guidance. Both of these haptic devices have a large workspace suitable for the range of human hand motion in skills training experiments.

The control loop runs at a rate of 1000 Hz, and the data is recorded at 30 Hz. The authority of the trainer over the trainee is higher than the authority of the trainee. This is provided by assigning a higher DC gain for H_{fh1} in (1.1). Giving more authority to the trainer will reduce the fatigue on her side making the teaching process easier.

3.3 Results

The performance measures used consist of the sample-by-sample error, the distance traveled and the completion time. Tables 3.1 and 3.2 list the root mean square error for subjects in both groups for the first and second segments of the path (see Fig. 3.2). The data is recorded immediately after the tenth trial for both training and control group. As previously mentioned, the subjects under training can choose to receive the training or go through a trial alone. The number of trails and training differs for each subject, however, on average they have more trials than training (an average of 6 trials compared to 4 trainings). This confirms their active participation in the process.

Using the method proposed in the data analysis section, the error for each sample of the desired trajectory averaged over subjects is shown in Fig. 3.5 for both the training and control groups. The training group shows a much better performance specially in the first segment of the path.

According to the results presented in Tables 3.2 and 3.5, a major improvement in the temporal behavior of the subjects in the training group is noticed compared to that of those in the control group. On average the overall performance in the trajectory following is better by 5 millimeters in the first and 3 millimeters in the

Table 3.1: The Experimental Results for the training group. L is the length traveled, t_1 is the completion time for the first segment of the path and t_2 is the traveling time of the second segment of the path.

Subject	t_1	t_2	RMS1(m)	RMS2(m)	L(m)
1	10.71	2.88	0.013749	0.005847	0.344
2	10.56	4.38	0.035209	0.008297	0.349
3	18.00	5.43	0.016482	0.005625	0.359
4	8.52	2.91	0.022225	0.006570	0.311
5	18.39	5.97	0.017197	0.005530	0.412
6	20.40	5.67	0.016121	0.007544	0.359
7	16.05	5.28	0.018696	0.008110	0.341
8	15.06	4.65	0.054746	0.007084	0.391
9	12.24	2.67	0.023966	0.012175	0.416
mean	14.45	4.43	0.024265	0.007420	0.365

Table 3.2: The Experimental Results for the Control group. L is the length traveled, t_1 is the completion time for the first segment of the path and t_2 is the traveling time of the second segment of the path.

Subject	t_1	t_2	RMS1(m)	RMS2(m)	L(m)
1	14.70	3.78	0.027374	0.012252	0.375
2	25.77	10.95	0.024308	0.011228	0.350
3	12.45	16.35	0.048380	0.017104	0.374
4	14.34	4.02	0.027633	0.012746	0.371
5	39.27	10.11	0.036091	0.008942	0.395
6	17.43	4.77	0.021872	0.008321	0.350
7	30.12	9.42	0.036968	0.010471	0.375
8	42.09	11.04	0.025687	0.005545	0.330
9	13.14	5.01	0.020187	0.011382	0.323
mean	23.26	8.38	0.029833	0.010887	0.360

second segment of the path for those who received the training. In Fig. 3.6, the number of users in different tracking error ranges are shown according to which the number of trained users in lower error ranges is more than untrained subjects which further confirms the effectiveness of the training. Therefore, collaborative haptic training improves both trajectory following and the task completion time, with the effect on the latter being more pronounced. According to the data in Tables 3.1 and 3.2 no significant difference is observed in the average length traveled between the two groups where the desired path length is 0.310m.

An inspection of Fig. 3.2 shows that the second segment of the task is easier to follow visually because a big part of it is on the surface facing the users. The subjects could monitor the penetration of the device into the sphere by slight wobbling on the surface. Due to the dominance of the visual feedback in this portion of the path, the effect of haptic training is less noticeable. Based on the results in Fig. 3.5, haptic-guidance is more effective in the first segment of the path where vision is less reliable, and the users have no choice but to rely on other sensing modalities to acquire information about the task.

3.3.1 Discussion

All the experimental scenarios prior to the final experimental design confirm the effectiveness of human-haptic guidance in improving the temporal response by reducing the task completion time. However, these experiments fail to capture any significant improvement in trajectory tracking accuracy of the subjects who

received haptic-guided training. The final experimental design , i.e. three dimensional curvy path, is the only scenario in which the training group performed better in following the desired trajectory. This improvement in trajectory tracking is most significant in the first segment of the path where vision is most defective. In the other prior experiment designs vision overshadows force and kinesthetic feedback, but in the last experiment the depth perception is missing which encourages the trainees to pay attention to the trainer's guidance. This shows that human-haptic guidance helps improve the training process by compensating for imperfections in the visual display of the 3D path.

Another interesting finding in the final experimental design is the effect of engaging the trainee in the training process. In this experiment at each stage of training, the trainee can choose whether she wants to receive the haptic training or to try the task herself. As a result, the trainee can benefit from the training as well as learning from her mistakes during the trials. This provides the trainee with the chance to be more attentive to the trainer's guide instead of being passively dragged around, and confirms the importance of active participation of the trainee in human-haptic training.

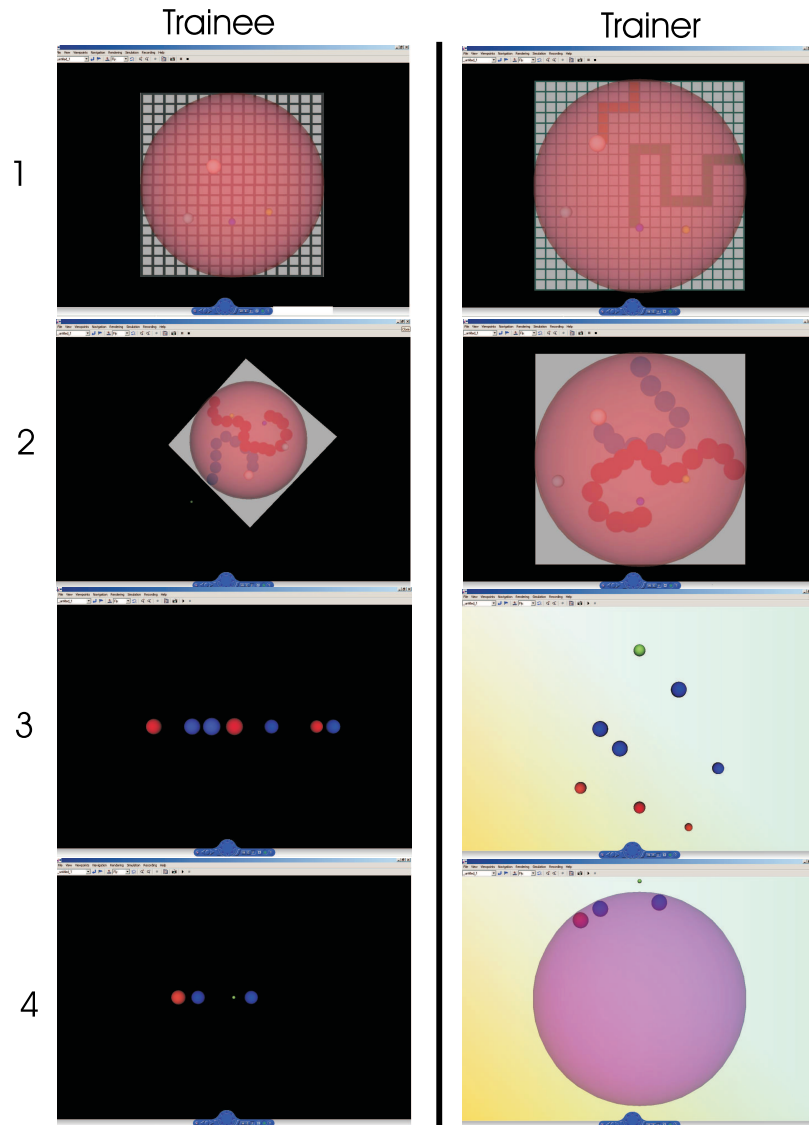


Figure 3.1: The virtual reality model displayed on trainee and trainer sides. 1. tumor removal grid-on, 2. tumor removal curvy path, 3. dimension reduction in the display, 4. combination of curvy path and dimension reduction.

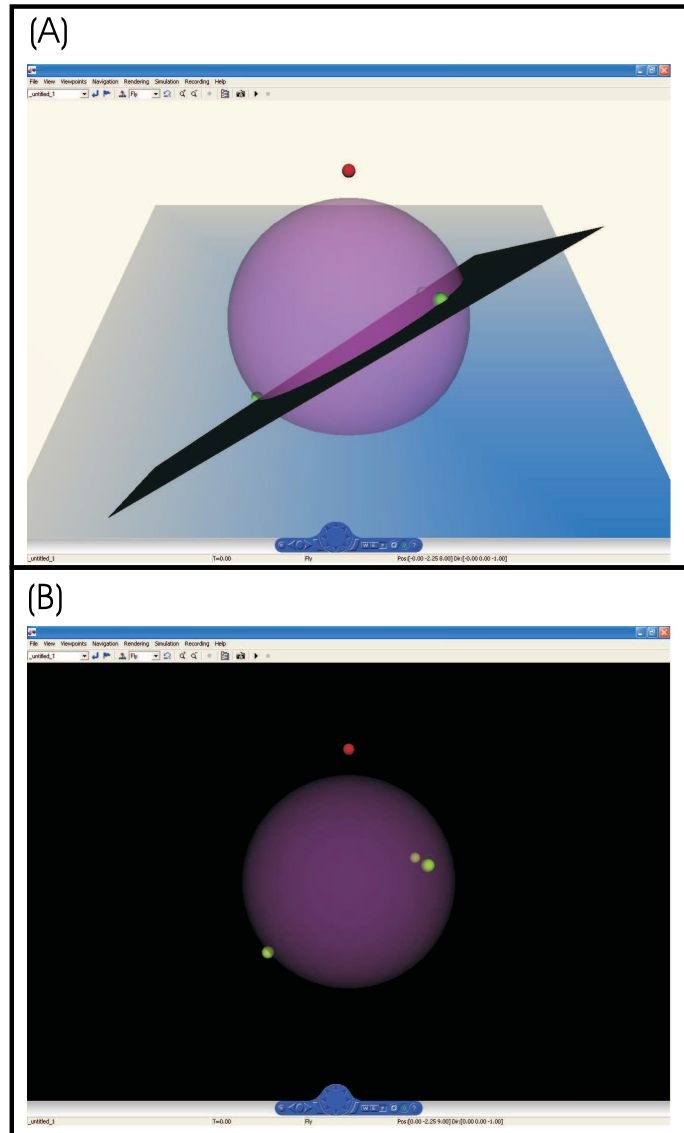


Figure 3.2: A) Virtual reality display on the trainer side, B) Virtual reality display on the trainee side. The red ball marks the user position and the green balls represent three targets distributed on the purple sphere. The users were instructed to move from left to right.

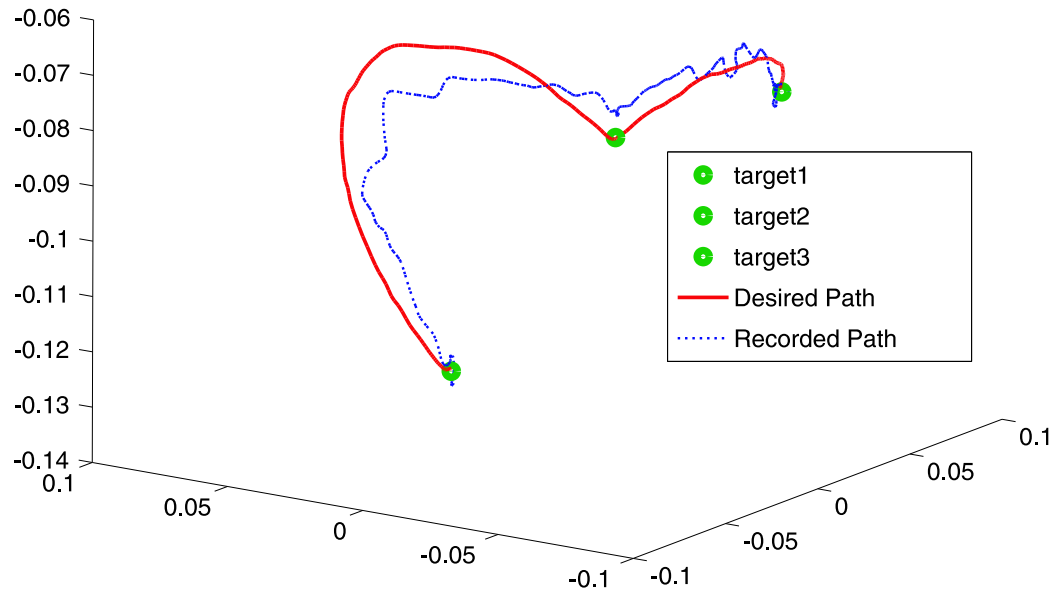


Figure 3.3: The desired and the actual path presented to one of the users after the trial. (The balls mark the targets.)

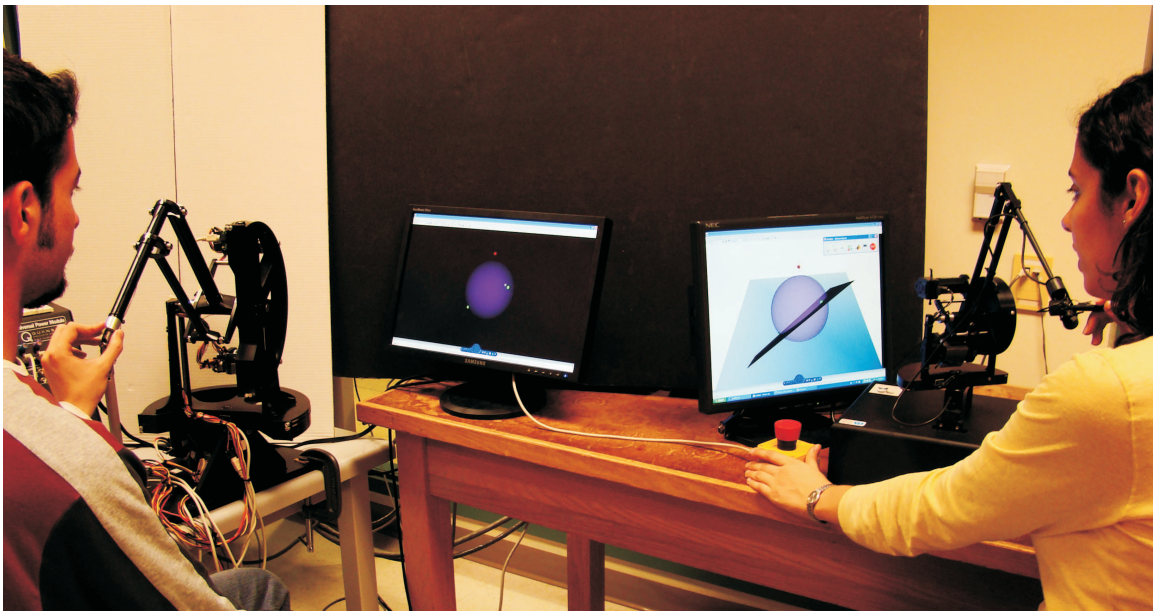


Figure 3.4: The experimental set-up.

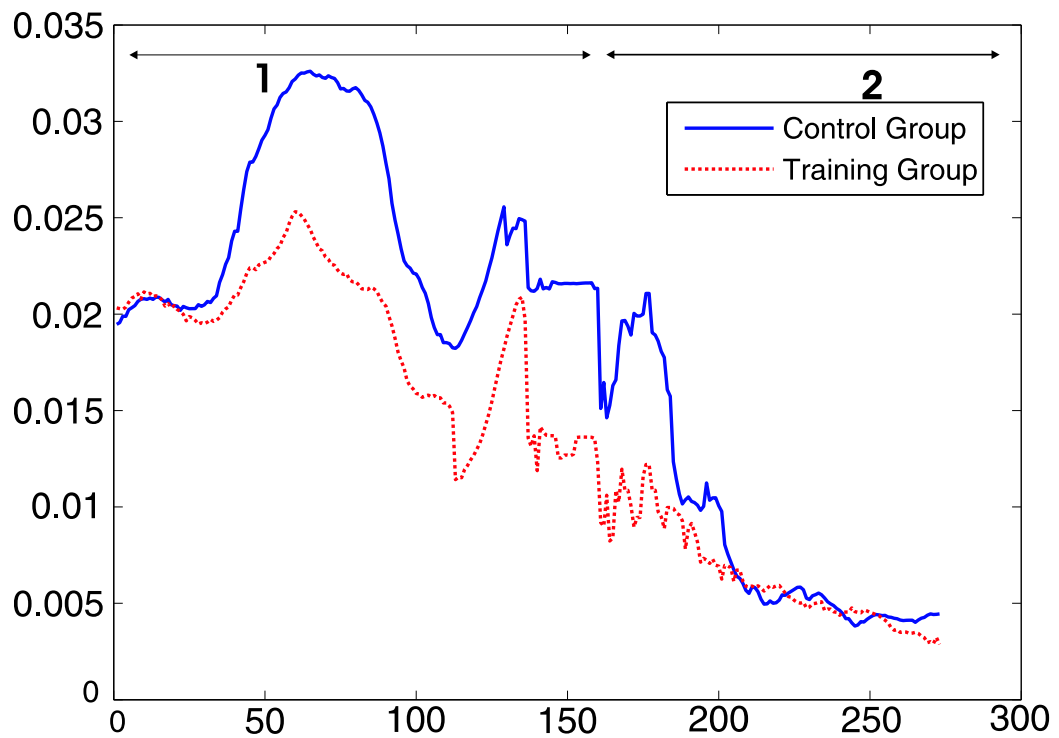


Figure 3.5: The mean error versus samples in the desired trajectory (The recorded desired trajectory consists of 273 samples. The first half of the path is marked with 1 and the second with 2).

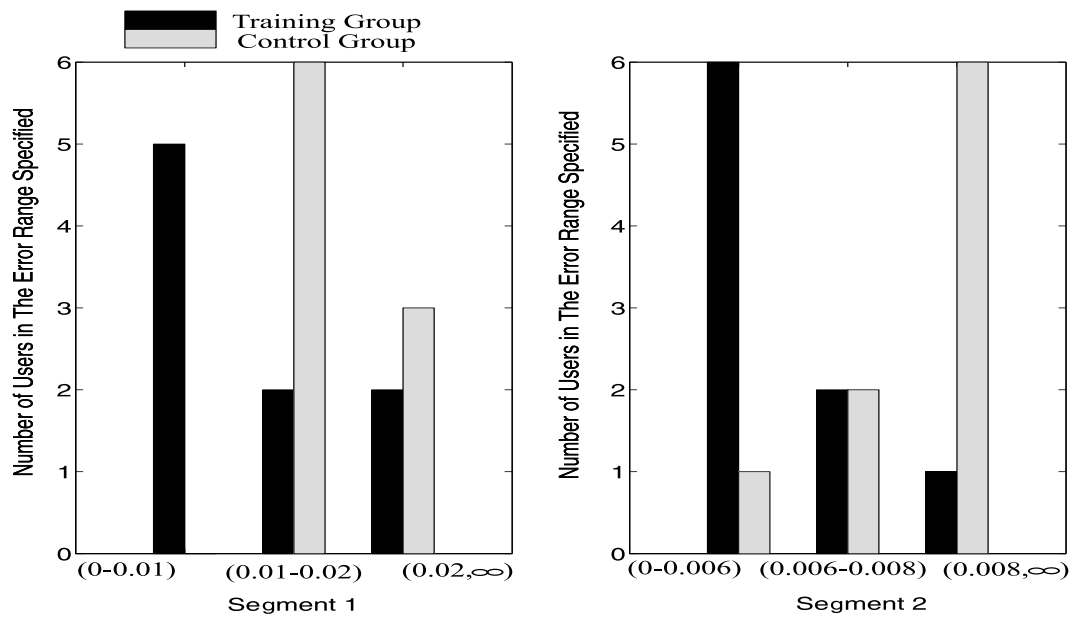


Figure 3.6: Number of users versus different error ranges in meters.

Chapter 4

Adaptive Controllers

Motivated by the results of the human factor studies in the previous chapter, a control framework is designed for realizing collaborative haptic training. This general control framework incorporates different force and position mappings which can be used to achieve different training goals such as workspace magnification and authority sharing between the users. Throughout this chapter the overall dynamics of the system are presented and the controller design for both impedance and admittance-type virtual environments is discussed in details. The design involves developing a trilateral control scheme for the realization of collaborative haptic training. The performance of the system in parameter approximation, and its ability to provide the requirements of a collaborative training framework is evaluated using a Lyapunov analysis .

4.1 System Dynamics

The dynamics of the haptic devices used by the trainer ($i = 1$), and the trainee ($i = 2$) are given by

$$D_{mi}(x_{mi}, t)\ddot{x}_{mi} + C_{mi}(x_{mi}, \dot{x}_{mi}, t)\dot{x}_{mi} + G_{mi}(x_{mi}, t) = F_{mi} - F_{ext,mi} \quad (4.1)$$

where x_{mi} denotes the device position in workspace coordinates, $D_{mi}(x_{mi})$ represents the mass matrix, $C_{mi}(x_{mi}, \dot{x}_{mi})$ embodies Coriolis and centrifugal effects, $G_{mi}(x_{mi})$ captures position-dependent forces such as gravity, F_{mi} is the device control force, and finally $F_{ext,mi}$ denotes external forces applied to the device end-effector. The following properties hold for the matrices introduced in (4.1) [44].

$$D_{mi}(x_{mi}) > 0, \text{ is positive definite and symmetric} \quad (4.2)$$

$$\dot{D}_{mi}(y) - 2C_{mi}(y, z) \quad \text{is skew symmetric}$$

It should be noted that the second property is only valid when Cristoffel symbols are used. Otherwise, $x^T(\dot{D}_{mi}(y) - 2C_{mi}(y, z))x = 0$ is satisfied just for $x = z$. The dynamics of user arms and environment are assumed to be second-order LTI models to avoid complicated modeling and analysis (4.3). This type of modeling has proven to provide satisfactory results in previous studies, e.g. see [9].

$$F_{ext,mi} = -F_{hi} = M_{hi}\ddot{x}_{mi} + B_{hi}\dot{x}_{mi} + k_{hi}(x_{mi} - x_{mi0}) - F_{hi}^* \quad (4.3)$$

where F_{hi}^* is a bounded exogenous force for user i . This model assumes the hand mass (M_{hi}) in conjunction with spring (k_{hi}) and damper (B_{hi}) effects for the human

operator. The overall dynamics of both human and haptic device can be lumped together in the following form

$$M_{mi}\ddot{x}_{mi} + C_{mi}\dot{x}_{mi} + G_{mi} = F_{cmi} + F_{hi}^* \quad (4.4)$$

$$M_{mi} = D_{mi}(x_{mi}) + M_{hi}$$

$$C_{mi} = C_{mi}(\dot{x}_{mi}, x_{mi}) + B_{mi}$$

$$G_{mi} = G_{mi}(x_{mi}) + K_{hi}[x_{mi} - x_{mi0}]$$

where F_{cmi} is the control force applied to the user specified by mi . It can be easily shown that in general $y^T (\dot{M}_{mi} - 2C_{mi}) y \leq 0$. In order to apply a monotonic non-linear function $k_p(\cdot)$, the first user's position can be mapped into new coordinates $k_p(x_{m1})$ resulting in the following dynamics

$$M'_{m1}\ddot{q}_{m1} + C'\dot{q}_{m1} + G'_{m1} = J^{-T}F_{m1} \quad (4.5)$$

$$M'_{m1} = J^{-T}M_{m1}J^{-1}$$

$$C'_{m1} = J^{-T}[C_{m1} - M_{m1}J^{-1}\dot{J}]J^{-1}$$

$$G'_{m1} = J^{-T}G_{m1}$$

where J is the Jacobian matrix, and

$$q_{m1} = k_p(x_{m1}) \quad (4.6)$$

$$\dot{q}_{m1} = \dot{k}_p(x_{m1}) = J\dot{x}_{m1}$$

$$\ddot{q}_{m1} = \ddot{k}_p(x_{m1}) = J\ddot{x}_{m1} + \dot{J}\dot{x}_{m1}$$

It can be shown that $y^T(\dot{M}'_{m1} - 2C'_{m1})y \leq 0$ still holds for non-singular Jacobian matrices.

4.2 Control Design

The general form of the control laws for interaction with both impedance and admittance-type virtual environments is given by

$$F_{cmi} = Y_{mi}(\dot{\rho}_{mi} + \ddot{x}_{mi}, \dot{x}_{mi}, \rho_{mi} + \dot{x}_{mi}, x_{mi})\hat{\Theta}_{mi} + k_{mi}\rho_{mi} - \alpha_{hi}\text{sgn}(\rho_{mi}) \quad (4.7)$$

where α_{hi} is an upper bound on $|F_{hi}^*|$, $\hat{\Theta}_{mi}$ is an estimation of the vector of unknown user and haptic device parameters Θ_{mi} with the estimation error defined as $\tilde{\Theta}_{mi} = \hat{\Theta}_{mi} - \Theta_{mi}$, and ρ_{mi} will be later defined for each environment type. Moreover, Y_{mi} is a known regressor matrix in the linear-in-parameter formulation of the combined user/device dynamics. For the admittance-type environment, and for the second($i=2$) user in the impedance-type environment configuration, $Y_{mi}\Theta_{mi}$ has the following form

$$Y_{mi}\Theta_{mi} = M_{mi}(x_{mi})\frac{d}{dt}(\rho_{mi} + \dot{x}_{mi}) + C_{mi}(x_{mi}, \dot{x}_{mi})(\rho_{mi} + \dot{x}_{mi}) + G_{mi}(x_{mi}) \quad (4.8)$$

whereas for the first ($i=1$) user in impedance-type environment, (4.8) is modified as follows to account for the nonlinear mapping $k_p(\cdot)$

$$\begin{aligned}
Y_{m1}\Theta_{m1} &= M'_{m1}(k_p(x_{m1}))\frac{d}{dt}(\rho_{m1} + \dot{k}_p(x_{m1})) \\
&\quad + C'_{m1}(k_p(x_{m1}), \dot{k}_p(x_{m1}))(\rho_{m1} + \dot{k}_p(x_{m1})) + G'_{m1}(k_p(x_{m1})) \quad (4.9)
\end{aligned}$$

The following adaptation laws are proposed for parameter estimation as in [9].

$$\dot{\hat{\Theta}}_{mip} = \begin{cases} 0, & \hat{\Theta}_{mip} \leq \Theta_{mip}^- \text{ and } Y_{mip}^T \rho_{mi} \leq 0 \\ 0, & \hat{\Theta}_{mip} \geq \Theta_{mip}^+ \text{ and } Y_{mip}^T \rho_{mi} \geq 0 \\ \Gamma_{mip}^{-1} Y_{mip}^T \rho_{mi}, & \text{otherwise} \end{cases} \quad (4.10)$$

where the index p refers to the p^{th} parameter for either m_1 or m_2 , Θ_{mip}^- and Θ_{mip}^+ denote the minimum and maximum values of the parameters, and Γ_{mip} is a matrix chosen to be strictly positive ($\Gamma_{mip} > 0$). The definitions of ρ_{m1} and ρ_{m2} for impedance and admittance-type environments will be presented later on.

Throughout the rest of this chapter where time domain quantities are implied, $H_{ind}u = L^{-1}\{H_{ind}(s)L\{u(t)\}\}$ for notational cleanliness, where H_{ind} is a transfer function, u denotes a time domain quantity and L is the Laplace operator. In addition, if R is one of the following $\{x_{mi}, \dot{x}_{mi}, k_p(x_{m1}), \dot{k}_p(x_{m1})\}$, $i = 1, 2$, then the notation \tilde{R} represents the following filtered quantity and its derivative

$$\mathbb{L}\{\tilde{R}\} = \frac{C}{s+C}L\{R\} \quad (4.11)$$

$$\dot{\tilde{R}} = CR - C\tilde{R} \quad (4.12)$$

4.2.1 Impedance-type Virtual Environments

The definitions of control variables ρ_{m1} and ρ_{m2} for impedance-type environments are inspired by some earlier work on adaptive bilateral teleoperation control for single-operator systems in [8,9]. The block diagram of the proposed control system is displayed in Fig. 4.1. Impedance-type virtual environments generate the environment reaction force based on the position of a virtual tool, which is often the measured position of the haptic device. In cooperative haptics, however, the trainer and trainee jointly hold the virtual tool and therefore, a mapped combination of the two haptic devices positions can be used as the tool position, i.e.

$$x_e = H_{x1}x_{m1} + H_{x2}x_{m2} \quad (4.13)$$

where H_{x1} and H_{x2} are strictly proper LTI filters. The environment reaction force is then given by:

$$f_e = k_e(x_e) \quad (4.14)$$

To enable cooperative haptics, the error signals ρ_{mi} in (4.7) are defined as follows:

$$\rho_{m1} = \nu_{m1d} - H'_{xm1}\dot{k}_p(x_{m1}) + AH_{fh1}f_h^1 \quad (4.15)$$

$$\rho_{m2} = \nu_{m2d} - H'_{xm2}\dot{x}_{m2} + AH_{fh2}f_h^2 \quad (4.16)$$

where

$$\begin{aligned} \nu_{m1d} = & H'_{xm2}\dot{\tilde{x}}_{m2} + \Lambda(H'_{xm2}\tilde{x}_{m2} - H'_{xm1}k_p(x_{m1})) \\ & + AH_{fh2}f_h^2 - Ak_f(H_{fe}f_e) \end{aligned} \quad (4.17)$$

and

$$\begin{aligned} \nu_{m2d} = & H'_{xm1} \dot{\tilde{k}}_p(x_{m1}) + \Lambda(H'_{xm1} \tilde{k}_p(x_{m1}) - H'_{xm2} x_{m2}) \\ & + AH_{fh1} f_h^1 - Ak_f(H_{fe} f_e) \end{aligned} \quad (4.18)$$

In(4.15)-(4.18), $k_p(\cdot)$ and $k_f(\cdot)$ are static nonlinear position and force mappings, respectively, $H'_{xmi} = 1 + H_{xmi}$, $i = 1, 2$; H_{xmi} , H_{fh1} , H_{fh2} , and H_{fe} are strictly proper LTI filters, and Λ and A are constant gains.

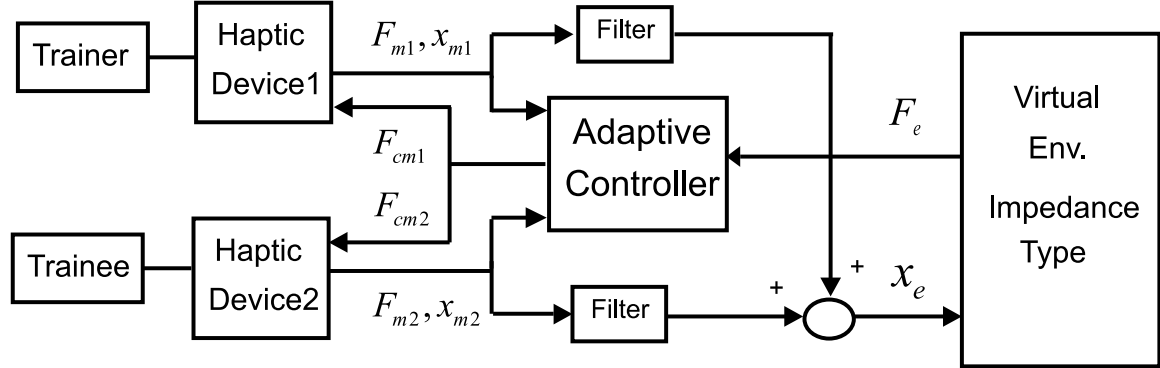


Figure 4.1: Cooperative haptics control with impedance-type virtual environment.

4.2.2 Admittance-type Virtual Environments

The block diagram of the proposed control system for admittance-type virtual environments is shown in Fig. 4.2. In admittance-type virtual environments, the displacement of the virtual environment is generated based on the user exerted force on the haptic device. In cooperative haptics, however, the trainer and trainee jointly hold the virtual tool and therefore, a mapped combination of the two users forces can be passed to the virtual environment simulator. An intervening mass-damper type tool is introduced to render the system well-defined in free motion

where the admittance of the environment is ill-defined.

$$f_e = H_{fe}^{-1} k_f^{-1} (H_{fh1} f_{h1} + H_{fh2} f_{h2} - H_{zt} x_e) \quad (4.19)$$

where

$$H_{zt} = \frac{s^2 + \Lambda s}{A(s + C)} \quad (4.20)$$

In this case, the tracking errors ρ_{mi} in (4.7) are defined as follows:

$$\rho_{m1} = \dot{k}_p^{-1} \left(\frac{x_e}{H'_{xm1}} \right) - \dot{x}_{m1} + \Lambda \left(k_p^{-1} \left(\frac{x_e}{H'_{xm1}} \right) - x_{m1} \right) \quad (4.21)$$

$$\rho_{m2} = \frac{\dot{x}_e}{H'_{xm2}} - \dot{x}_{m2} + \Lambda \left(\frac{x_e}{H'_{xm2}} - x_{m2} \right) \quad (4.22)$$

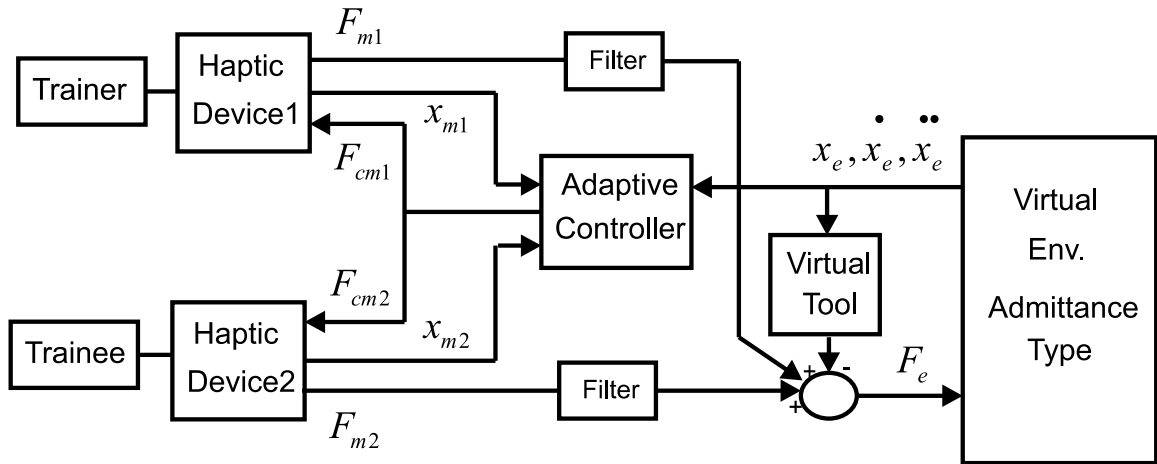


Figure 4.2: Cooperative haptics control with admittance-type virtual environment.

4.2.3 Performance analysis

To demonstrate how the proposed controllers coordinate the users and the virtual environment, the following candidate Lyapunov function is defined

$$V_m = \sum_{i=1,2} \frac{1}{2} \rho_{mi}^T M_{mi} \rho_{mi} + \hat{\Theta}_{mi}^T \Gamma_{mi} \tilde{\Theta}_{mi} \quad (4.23)$$

where M_{mi} is defined in (4.4) and $\Gamma_{mi} > 0$. Substituting the control force in (4.7) into the system dynamics in (4.4) yields

$$-Y_{mi} \tilde{\Theta}_{mi} = M_{mi} \dot{\rho}_{mi} + C_{mi} \rho_{mi} + k_{mi} \rho_{mi} + F_{hi}^* - \alpha_{hi} \text{sign}(\rho_{mi}) \quad (4.24)$$

Taking the derivative of (4.23) along the closed-loop dynamics in (4.4) and using the adaptation law (4.10) result in

$$\dot{V}_m \leq \sum_{i=1,2} -\rho_{mi}^T k_{mi} \rho_{mi} \quad (4.25)$$

Using (4.23) and (4.25) it can be concluded that

$$\rho_{mi} \in L_2 \cap L_\infty, i = 1, 2 \quad (4.26)$$

It can also be shown that ρ_{mi} converges to zero as in [9, 24]. Later in this chapter, the aforementioned properties of ρ_{mi} will be used for achieving the transparency objectives.

Impedance-type virtual environments

Subtracting (4.16) from (4.15) and substituting from (4.17) and (4.18) yield

$$\begin{aligned} \rho_{m1} - \rho_{m2} &= H'_{xm2} \dot{\tilde{x}}_{m2} - H'_{xm1} \dot{k}_p(x_{m1}) - H'_{xm1} \dot{\tilde{k}}_p(x_{m1}) \\ &+ H'_{xm2} \dot{x}_{m2} + \Lambda(H'_{xm2} \tilde{x}_{m2} - H'_{xm1} k_p(x_{m1}) - H'_{xm1} \tilde{k}_p(x_{m1}) + H'_{xm2} x_{m2}) \end{aligned} \quad (4.27)$$

It can be seen that (4.27) is in the form of $u = \dot{y} + cy$ and therefore Lemma 1 from [9] can be applied to obtain

$$\rho_e = H'_{xm2} x_{m2} - H'_{xm1} k_p(x_{m1}) \in L_2 \cap L_\infty \quad (4.28)$$

$$\rho_p = H'_{xm2} \dot{x}_{m2} - H'_{xm1} \dot{k}_p(x_{m1}) \in L_2 \cap L_\infty \quad (4.29)$$

Adding (4.15) and (4.16) results in

$$\begin{aligned} \rho_{m1} + \rho_{m2} &= 2A(H_{fh1} f_h^1 + H_{fh2} f_h^2 - k_f(H_{fe} f_e)) \\ &- C^{-1}[H'_{xm2} \ddot{\tilde{x}}_{m2} + H'_{xm1} \ddot{\tilde{k}}_p(x_{m1}) \\ &+ \Lambda(H'_{xm2} \dot{\tilde{x}}_{m2} + H'_{xm1} \dot{\tilde{k}}_p(x_{m1}))] \end{aligned} \quad (4.30)$$

which can be written in the form of

$$H_{fh1} f_h^1 + H_{fh2} f_h^2 - k_f(H_{fe} f_e) - \bar{\rho} = \frac{s^2 + \Lambda}{CA} \tilde{x}_{m2} H'_{xm2} = H_{zt} H'_{xm2} x_{m2} \quad (4.31)$$

where

$$\bar{\rho} = \frac{1}{2A}[\rho_{m1} + \rho_{m2} - C^{-1}(s + \Lambda)\tilde{\rho}_p] \in L_2 \cap L_\infty \quad (4.32)$$

Note that (4.28) and (4.29) show the establishment of a generalized position tracking between the two users characterized by the LTI filters H'_{xm1} and H'_{xm2} and the static nonlinear mapping $k_p(\cdot)$. Moreover, (4.31) demonstrates a generalized mixed linear/nonlinear mapping enforced between the users and environment forces which is characterized by H_{f1} , H_{f2} , H_{fe} , and $k_f(\cdot)$. An adjustable intervening impedance in the form of H_{zt} also appears in (4.31). The intervening tool mass and damping can be tuned through changes in C , A and Λ . The block diagram of the resulting closed-loop system is shown in Fig. 4.3 where f_{hi}^* denotes the human exogenous force for user i .

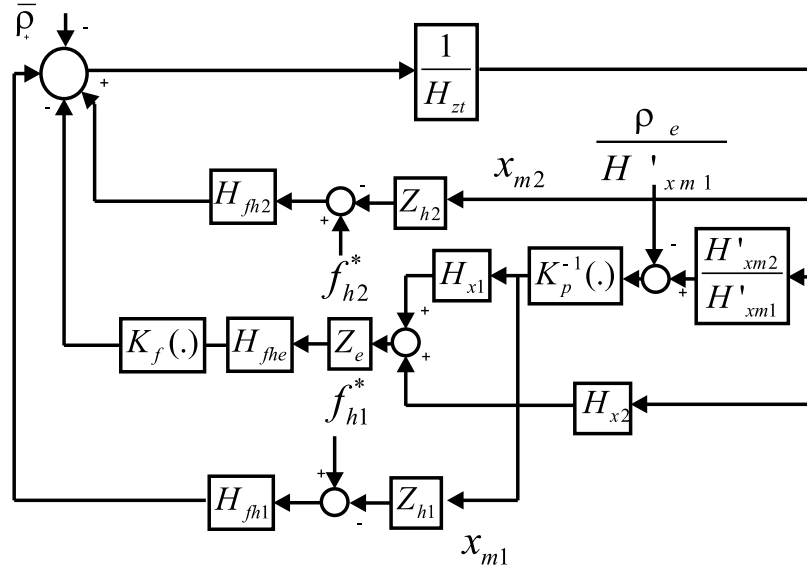


Figure 4.3: Closed-loop system for impedance-type environments.

Admittance-type virtual environments

In this case of an admittance-type virtual environment, a generalized position tracking in the form of (4.28) directly follows from (4.21) and (4.22). In particular by defining $\rho_{e1} = k_p^{-1}(\frac{x_e}{H'_{xm1}}) - x_{m1}$, $\rho_{e2} = \frac{x_e}{H'_{xm2}} - x_{m2}$ and $\rho_{pi} = \dot{\rho}_{ei}$, it can be shown that $\rho_{ei}, \rho_{mi} \in L_2 \cap L_\infty$. The generalized force tracking behavior can be deduced from (4.19) by replacing x_e from (4.22). Fig. 4.4 features the block diagram of the closed-loop system with the controller for an admittance-type virtual environment.

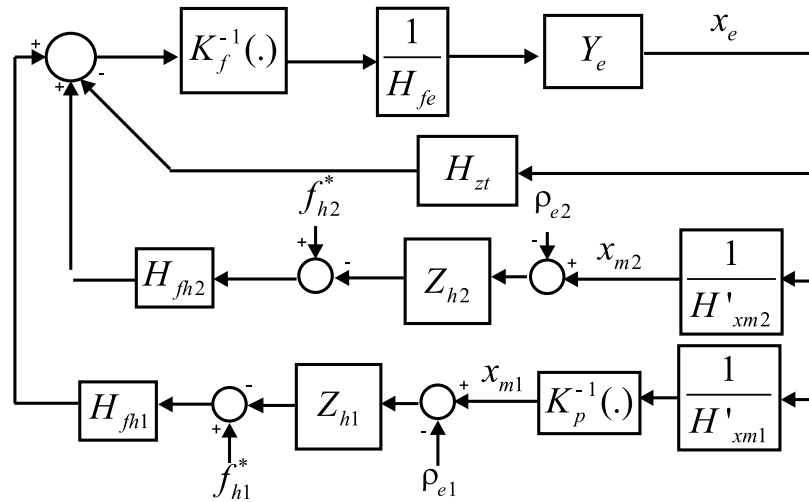


Figure 4.4: Closed-loop system for admittance-type environments.

Chapter 5

Robust Control Analysis

The proposed adaptive controllers ensure that the desired generalized force and position tracking in the collaborative haptic training framework are achieved. However, there are still uncertainties in the resulting closed-loop control system in the form of uncertainty in the users and environment parameters that affect the stability of the overall system. This chapter focuses on investigating the stability of the closed-loop system in the presence of user and environment uncertainties. A robust stability analysis for different filter parameters is carried out. First the case of sheer LTI filters is addressed for a family of transfer functions resulting from boundary conditions on the uncertainties. Next, the stability of the system is evaluated in the presence of nonlinear position or force mappings.

The analysis in this chapter is based on the closed-loop representation of the system for impedance and admittance environment types developed in the previous section. The block diagram of the system developed is shown in Figs. 5.1 and 5.2.

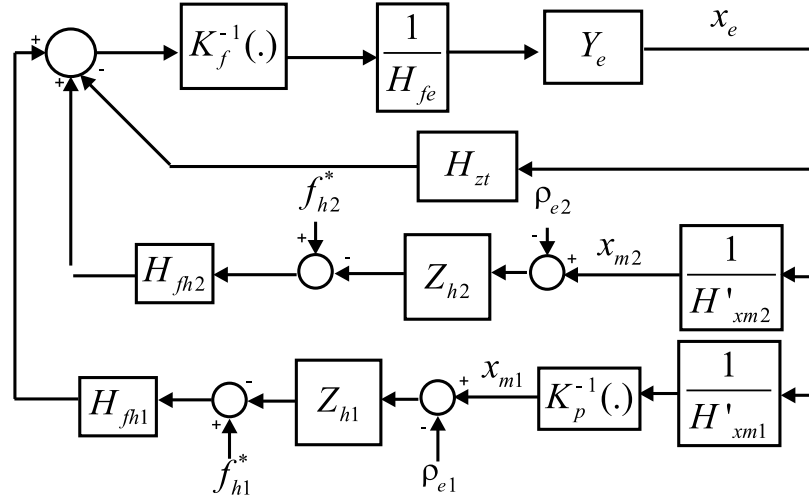


Figure 5.2: Closed-loop system for admittance-type environments.

polynomials result from the boundary condition on the uncertainties. As the set of polynomial roots change continuously, the stability is guaranteed only when $c(j\delta, q) \neq 0$. This requires that the origin of the complex plane be excluded from the convex hull formed by the extremal polynomials [45]

For polynomials with linearly dependent coefficients, a more general form of analysis is required. According to Barmish [46], at a fixed frequency the extremal points of the family of the polynomials define a convex hull representing the image set formed by changing the unknown coefficients within their bounds. The roots of all polynomial family members are on the left hand side of imaginary axis if and only if the resulting polygon does not include the origin [46,47]. As proposed in [7], zero exclusion property can be checked by a process based on maximum phase difference. If each of the edge polynomials forming the vertex of the polygon is denoted by $C_{E_i}(jw)$ and any other edge by $C_{E_*}(jw)$, the following process rotates

the convex hull to intersect the real axis. Defining

$$\Phi_{C_{E_i}} = \text{phase}(\Phi_{C_{E_i}}(jw)) - \text{phase}(\Phi_{C_{E_*}}(jw)) + 2k\pi \quad (5.2)$$

where

$$k = \begin{cases} -1, & \text{phase}(C_{E_i}(jw)) - \text{phase}(C_{E_*}(jw)) < -\pi \\ 1, & \text{phase}(C_{E_i}(jw)) - \text{phase}(C_{E_*}(jw)) > \pi \\ 0, & \text{otherwise} \end{cases} \quad (5.3)$$

yields

$$-\pi \leq \Phi_{C_{E_i}}(w) \leq \pi \quad (5.4)$$

The origin is excluded from the convex hull if

$$\sup_{w \in R^+} [\max_i \Phi_{C_{E_i}}(w) - \min_i \Phi_{C_{E_i}}(w)] < \pi \quad (5.5)$$

In the stability analysis, users hand dynamics are modeled as mass-spring-damper impedances. Impedance-type environments are only modeled as spring-dampers since modeling mass would require the acceleration measurement of the haptic devices. The admittance-type environments, however, can involve all three parameters, i.e. mass, damping, and stiffness. An arbitrary set of parameter ranges given in Table 5.1 was chosen to perform the stability analysis for a number of different cases.

For the impedance-type environment control, the block diagram depicted in Fig. 5.1 can be transformed into Fig. 5.3 where u is formulated as

$$u = H_{fh2}f_h^{2*} + H_{fh1}f_h^{1*} - \bar{\rho} + \frac{\rho_e}{k_p H'_{xm1}} [z_{h1} H_{fh1} + H_{x1} z_e k_f H_{fe}] \quad (5.6)$$

Table 5.1: Parameter Boundaries

	<i>Environment</i>	<i>User1</i>	<i>User2</i>
<i>mass(m)</i>	0.676-0.866	0-0.3	0-0.3
<i>damper(b)</i>	5-50	0-100	0-100
<i>spring(k)</i>	10-1000	20-1000	20-1000

The resulting characteristic function would then be in the form of

$$C(s) = A(s + C)(k_p H'_{xm1} H_{fh2} z_{h2} + H'_{xm2} (H_{fh1} z_{h1} + k_f H_{fe} z_e H_{x1}) + k_f H_{fe} H_{x2} z_e k_p H'_{xm1}) + (s^2 + s\Lambda) H'_{xm2} H'_{xm1} k_p \quad (5.7)$$

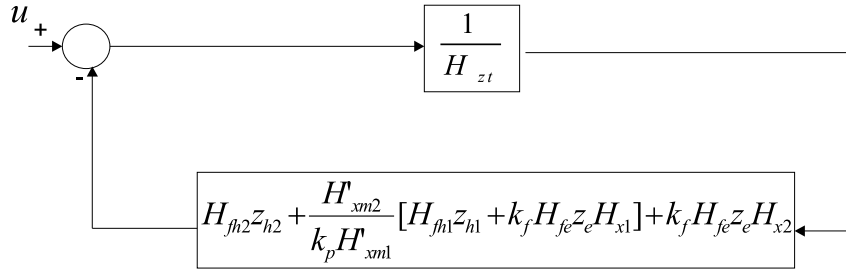


Figure 5.3: Closed-loop system for impedance-type environments when all filters are LTI.

For the admittance-type environment control presented in Fig. 5.2, the block diagram can be transformed into Fig. 5.4 where u is formulated as (5.8).

$$u = f_h^1 H_{fh1} + f_h^2 H_{fh2} \quad (5.8)$$

Using the block diagram in Fig.(5.4) results in the following characteristic function

$$c(s) = A(s + C)(k_f H_{fe} k_p H'_{xm1} H'_{xm2} z_e + H'_{xm2} H_{fh1} z_{h1} + k_p H'_{xm1} H_{fh2} z_{h2}) + k_p H'_{xm1} H'_{xm2} (s^2 + s\Lambda) \quad (5.9)$$

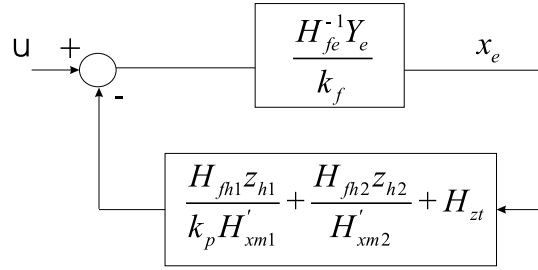


Figure 5.4: Closed-loop system for admittance-type environments when all filters are LTI.

5.1.1 Case 1: $\frac{H_{fhe}}{H_{fhi}}$

According to the general force mapping equation in (4.31), the feel of the user from the virtual environment can be modified using the ratio $\frac{H_{fhe}}{H_{fhi}}$. For instance, it might be desirable to increase this ratio at higher frequencies for the trainee so that high-frequency environment forces are better perceived. The following choices of filters would provide this effect when $\tau_2 > \tau_1$ (trainee is denoted with index $i = 2$):

$$H_{xm1} = H_{xm2} = 1, H_{fh1} = H_{fe} = \frac{c}{s + c} \quad (5.10)$$

$$H_{fh2} = \frac{c(\tau_1 s + 1)}{(s + c)(\tau_2 s + 1)}, k_f = k_p = 1$$

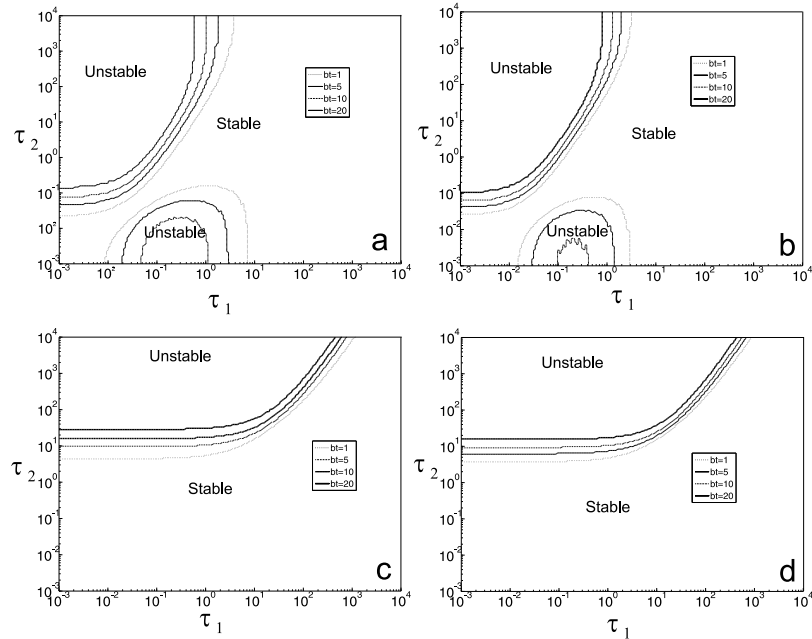


Figure 5.5: Stability regions with respect to τ_1 and τ_2 : (a) Impedance-type environment in Case 1; (b) Admittance-type environment in Case 1; (c) Impedance-type environment in Case 2; (d) Admittance-type environment in Case 2.

Using these filters, the coefficients of the characteristic equation of the closed-loop system for both virtual environments in Fig. 5.1 and Fig. 5.2 can be easily calculated.

Figs. 5.5.a, and 5.5.b depict the stability regions with respect to τ_1 and τ_2 and for different values of virtual tool damping b_t , for the impedance and admittance-type environments, respectively. The results were obtained by means of the zero exclusion test introduced earlier. It is worth noticing that decreasing the tool damping would clearly reduce the guaranteed stability region.

5.1.2 Case 2: $\frac{H_{fh1}}{H_{fh2}}$

The frequency depended ratio $\frac{H_{fh1}}{H_{fh2}}$ can be chosen such that the relative authority of the trainer ($m = 1$) is increased at low frequencies where most of hand voluntary motion occurs. This may be achieved through the following mapping filters when choosing $\tau_2 > \tau_1$:

$$\begin{aligned} H_{xm1} = H_{xm2} = 1, H_{fh1} = H_{fe} = \frac{c}{s + c} \\ H_{fh2} = \frac{c(s + \tau_1)}{(s + c)(s + \tau_2)}, k_f = k_p = 1 \end{aligned} \quad (5.11)$$

The coefficients of the closed-loop characteristic equation for the system can be obtained similarly. Figs. 5.5.c and 5.5.d show the region of guaranteed stability for the impedance and admittance-type virtual environment with respect to τ_1 and τ_2 for different values of virtual tool damping.

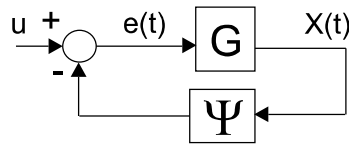


Figure 5.6: Nonlinear Luré feedback form.

5.2 Nonlinear Mapping

In order to analyze the stability including nonlinear mappings, the system block diagram can be transformed into a standard Luré feedback form depicted in Fig. 5.6 where Ψ is a nonlinear element and $G(s)$ is a linear rational transfer function [48]. There are a number of sufficient stability tests for such systems in the literature.

Among these is an off-axis circle criteria proposed in [49]. In this paper, the authors argue that for incrementally monotonic nonlinearities $\Psi(\cdot)$ satisfying

$$K_1 \leq \frac{\Psi(x_1) - \Psi(x_2)}{x_1 - x_2} \leq K_2 \quad (5.12)$$

if $G(j\omega)$ is completely outside a circle passing through $(-\frac{1}{K_2} + \delta, 0)$, and $(-\frac{1}{K_1} - \delta, 0)$, ($\delta > 0$) and it does not encircle it, then the system is asymptotically stable. As proposed in [8] using a bilinear transformation, this geometrical test can be replaced by the following equivalent condition

$$H(s) = \frac{G(s) + \frac{1}{2}(\frac{1}{K_1} + \frac{1}{K_2}) - dj - r}{G(s) + \frac{1}{2}(\frac{1}{K_1} + \frac{1}{K_2}) - dj + r} \quad (5.13)$$

$$r = \sqrt{d^2 + \frac{1}{4}(\frac{1}{K_1} - \frac{1}{K_2})^2}$$

$$\inf_{w \in R^+} \text{Re}(H(jw)) > 0 \quad (5.14)$$

where d is the center of the circle ($d \in R$). To determine stability, it suffices to show the validity of (5.14) for at least one arbitrary d . For $d = 0$ the test reduces to the conventional on-axis circle criteria which evidently may fail to identify some stable regions due to its conservatism.

The stability analysis in this case should also take into account the uncertainties present in the users and environment dynamics resulting in an uncertain linear plant $G(s)$. Hollot [50] argues that for all Hurwitz stable transfer functions $G(s)$ in the form of $\frac{N(s,q)}{D(s,q)}$ with the coefficients of numerator and denominator being independent of each other and having independent coefficients themselves, the Nyquist envelop of the plants is contained in the envelop of corresponding

Kharitonov plants. The term Kharitonov plants refers to any set of plants in the form $\frac{N_m(s,q)}{D_n(s,q)}$ with $N_m(s,q)$ and $D_n(s,q)$ as Kharitonov polynomials. If (5.1) has bounded real coefficients as $\underline{\gamma}_i \leq a_i \leq \bar{\gamma}_i$, the four Kharitonov polynomials are defined as [51]

$$\begin{aligned}\kappa_F^1(s) &= \underline{\gamma}_0 + \underline{\gamma}_1 s + \bar{\gamma}_2 s^2 + \bar{\gamma}_3 s^3 + \dots \\ \kappa_F^2(s) &= \underline{\gamma}_0 + \bar{\gamma}_1 s + \bar{\gamma}_2 s^2 + \underline{\gamma}_3 s^3 + \dots \\ \kappa_F^3(s) &= \bar{\gamma}_0 + \underline{\gamma}_1 s + \underline{\gamma}_2 s^2 + \bar{\gamma}_3 s^3 + \dots \\ \kappa_F^4(s) &= \bar{\gamma}_0 + \bar{\gamma}_1 s + \underline{\gamma}_2 s^2 + \underline{\gamma}_3 s^3 + \dots\end{aligned}\tag{5.15}$$

The original closed-loop systems can be transformed into their equivalent Luré feedback form shown in Fig. 5.6 for both impedance and admittance-type virtual environments so that the input u is in L_∞ . The nonlinear element Ψ is $k_f(\cdot)$ and $k_f^{-1}(\cdot)$ for the impedance and admittance-type environments, respectively. The transformations also result in

$$G_{\text{imp}}(s) = \frac{H_{fe} z_e (k_p H'_{xm1} H_{xm2} + H_{xm1} H'_{xm2})}{H_{zt} k_p H'_{xm1} + H_{fh2} z_{h2} k_p H'_{xm1} + z_{h1} H_{fh1} H'_{xm2}}\tag{5.16}$$

and

$$G_{\text{adm}}(s) = \left(\frac{H_{fh1} z_{h1}}{k_p H'_{xm1}} + \frac{H_{fh2} z_{h2}}{H'_{xm2}} + H_{zt} \right) Y_e H_{fe}^{-1}\tag{5.17}$$

open-loop transfer functions for both environment types. Figs. 5.7 and 5.8 depict the general block diagrams of the system transformed into the Luré form for impedance and admittance-type environments respectively.

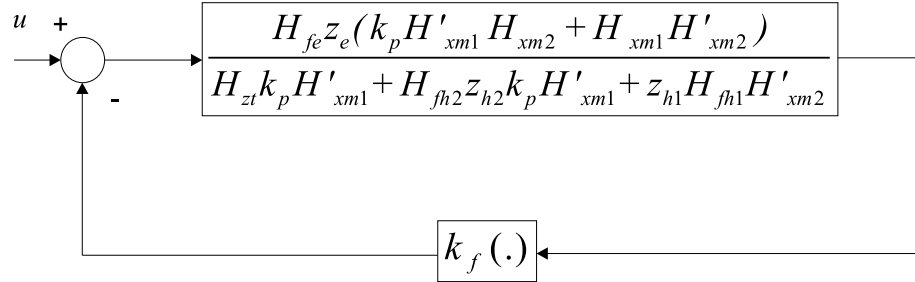


Figure 5.7: Closed-loop control system for interaction with a impedance-type environment transformed into nonlinear Luré form with $k_f(\cdot)$ as the nonlinear element.

$$u = f_h^{2*} H_{fh2} + f_h^{1*} H_{fh1} - \bar{\rho} + \frac{\rho e^{(1-H_{x2})}}{H'_{xm2}} (H_z t + H_{fh2} z_{h2})$$

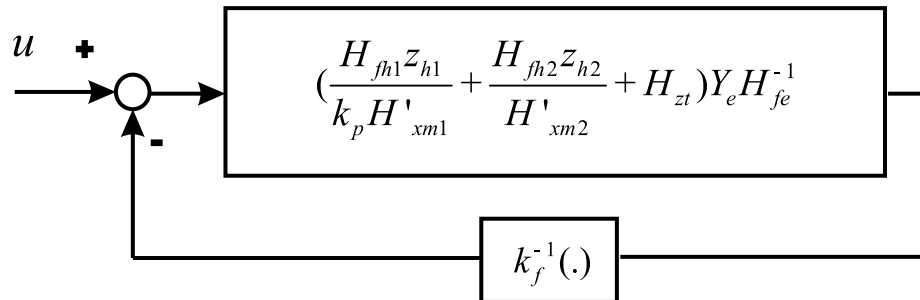


Figure 5.8: Closed-loop control system for interaction with an admittance-type environment transformed into nonlinear Luré form with $k_f(\cdot)$ as the nonlinear element.

$$u = \frac{f_h^1 H_{fh1} + f_h^2 H_{fh2}}{\left(\frac{H_{fh1} z_{h1}}{k_p H'_{xm1}} + \frac{H_{fh2} z_{h2}}{H'_{xm2}} + H_{zt} \right) Y_e}$$

It should be noted that only one nonlinear mapping element can be considered at a time. Here the results for a nonlinear force mapping $k_f(\cdot)$ and a constant gain position mapping k_p are given. Similar analysis can be carried out for constant gain force mapping k_f and a nonlinear position mapping $k_p(\cdot)$. In this case the open-loop transfer function can be formulated as follows

$$G_{\text{imp}}(s) = \frac{H'_{xm2}}{H'_{xm1}(H_{zt} + H_{fh2}z_{h2} + z_e)} \quad (5.18)$$

and

$$G_{\text{adm}}(s) = \frac{z_{h1}H_{fh1}H_{fe}Y_e}{H'_{xm1}(1 + H_{fe}Y_e(\frac{H_{fh2}z_{h2}}{H'_{xm2}} + H_{zt}))} \quad (5.19)$$

for impedance and admittance-type virtual environments. Figs. 5.9 and 5.10 depict the general block diagrams of the system transformed into the Luré form for impedance and admittance-type environments respectively with $k_p(\cdot)$ as the nonlinear mapping.

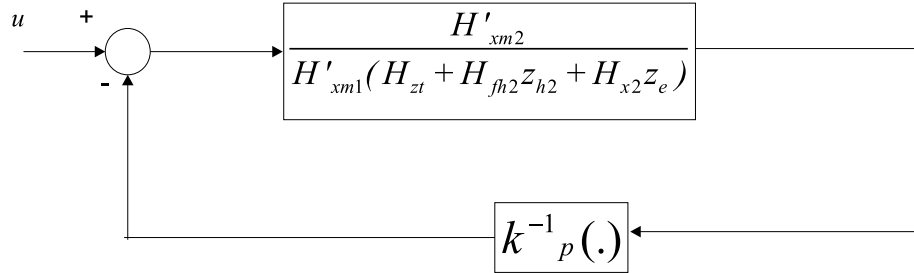


Figure 5.9: Closed-loop control system for interaction with an impedance-type environment transformed into nonlinear Luré form with $k_p(\cdot)$ as the nonlinear element. $u = \frac{1}{H_{fh1}z_{h1} + H_{x1}z_e} (f_h^{2*} H_{fh2} + f_h^{1*} H_{fh1} - \bar{\rho} + \frac{\rho_e}{H'_{xm1}} (H_{x1}z_e + H_{fh1}z_{h1}))$

The results of robust stability analysis using the envelop and 16 kharitonov plants is presented in Figs.5.11 and 5.12. It should be noted that the choices of the filters in the analysis has rendered the coefficients of $N_m(s, q)$ and $D_n(s, q)$ all

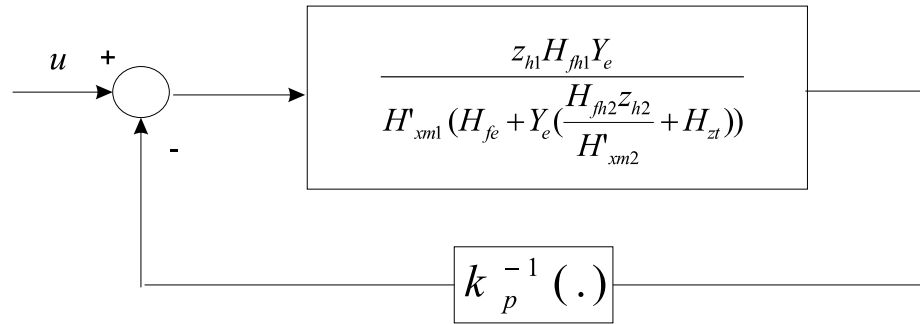


Figure 5.10: Closed-loop control system for interaction with an admittance-type environment transformed into nonlinear Luré form with $k_p(\cdot)$ as the nonlinear element. $u = \frac{f_h^1}{z_{h1}} + \frac{f_h^2 H_{fh2}}{z_{h1} H_{fh1}}$

independent. However, in the case where $N_m(s, q)$ and $D_n(s, q)$ are independent but any of them have dependent coefficients within their polynomials the same approach can be used. The only difference emerges in finding the boundaries of the Nyquist envelope where instead of Kharitonov plants extremal plants [47] applying edge theorem [52] is required [7].

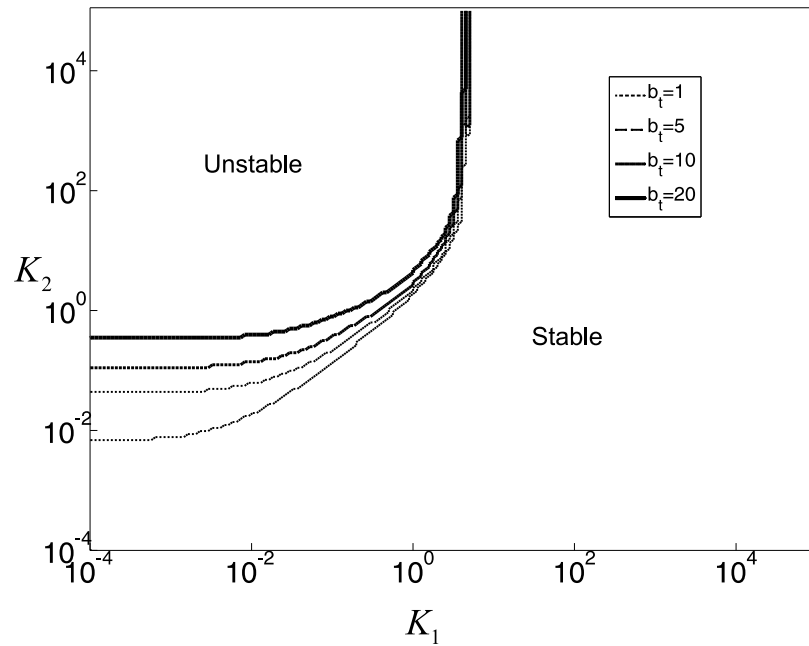


Figure 5.11: The result of stability analysis for impedance-type for various tool damping values with nonlinear mapping sectors.

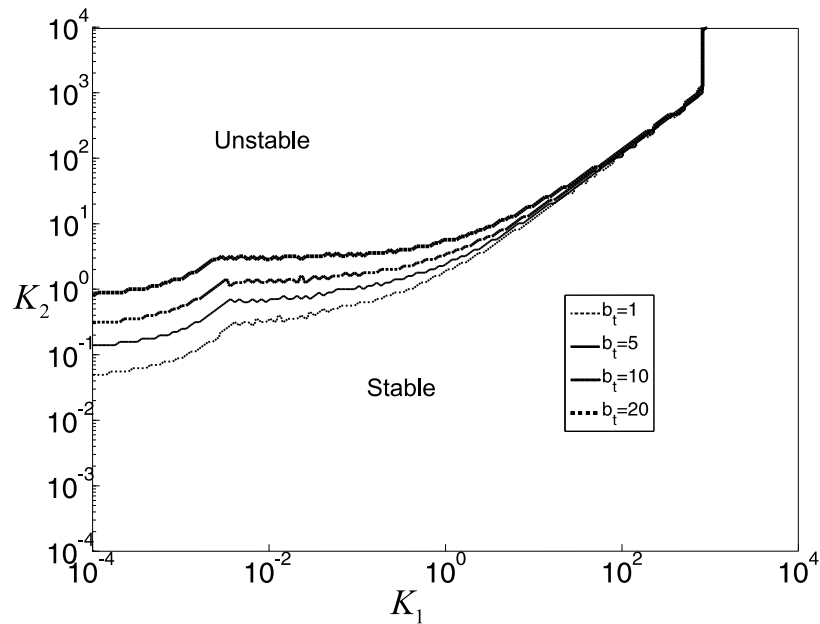


Figure 5.12: The result of stability analysis for admittance-type for various tool damping values with nonlinear mapping sectors.

Chapter 6

Experimental results

The ability of the proposed control framework to realize collaborative haptic training successfully needs to be tested. In this chapter experiments investigating the performance of the proposed system to initiate and maintain a stable collaborative control method are conducted using a virtual wall benchmark as the environment. The experimental setup is first explained in details. The experimental results are next presented for impedance and admittance environment types.

Table 6.1: Control Parameters

C	A	Λ	$\Gamma_1 = \Gamma_2$	$k_{m1} = k_{m2}$
150	0.01	15	[50 350 500]	50

6.1 Experimental Setup

The experimental setup shown in Fig. 6.1 consists of two similar Quanser twin-pantograph haptic devices each with two degrees of freedom along x and y axes. The devices are actuated by direct drive DC motors and the motor shaft angles are measured by optical encoders with 20,000 counts per revolution. The users interaction forces are directly measured by ATI Industrial Automation Mini40 force/torque sensors whereas the velocities are obtained by filtering the position signals. Matlab RTW/Tornado RTOS with a sampling rate of 1024Hz is employed to implement the controller.

The virtual environment in both impedance and admittance-type simulations is a spring-damper wall with which the users can make contact. To avoid chattering in the control signal due to the switching $\text{sign}(\cdot)$ element in the control action in (4.7), the user exogenous force F_{hi}^* is treated as one of the parameters to be estimated by the adaptation routine. This would provide satisfactory results in practice as the rate of change in F_{hi}^* is much slower than the adaptation speed. The control parameters for both environment types are presented in Table 6.1.

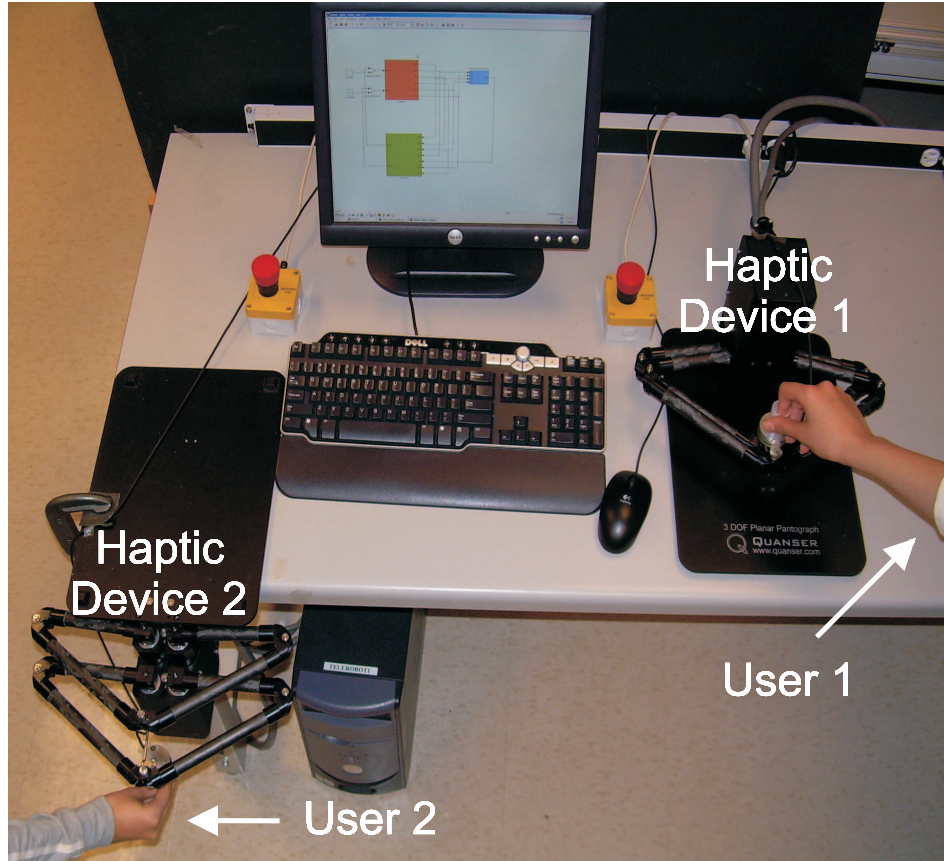


Figure 6.1: Experimental Setup

6.2 Impedance-type Environment

Figs. 6.2 and 6.3 present experimental results using the filters and gains listed in Table 6.2. In the nonlinear case, the force mapping $k_f(f_e) = \text{sgn}(F_e) \frac{f_e^2}{8}$ is substituted for the $k_f = 1$ used in the linear case. This nonlinear force mapping satisfies the condition given in [7] for improved environment stiffness perception.

For the impedance-type virtual environment, the wall has a stiffness of $2000 \frac{N}{M}$, and a damping of $10 \frac{N.s}{m}$. The proposed controller establishes a rigid link between

Table 6.2: Assigned Filters

	$\frac{H_{fh1}}{C}$	$\frac{H_{fh2}}{C}$	$\frac{H_{fe}}{C}$	K_p	$H_{x1} = H_{x2}$
<i>Impedance - type</i>	$\frac{1}{s+C}$	$\frac{1}{s+C}$	$\frac{1}{s+C}$	1	0.5
<i>Admittance - type</i>	0.25	0.75	1	1	0.5

the users through which they can interact with each other and the virtual wall. As shown in Figs. 6.2 and 6.3, the users are successfully following each other in both free motion and in contact with the wall. The adaptation routine is also providing satisfactory results. The third diagram in each of the figures confirms the ability of the system to provide force tracking (4.31). The difference between $H_{fh1}f_h^1 + H_{fh2}f_h^2$ and $H_{fe}f_e$ is due to the intervening tool dynamics.

6.3 Admittance-type Environment

The filters are again assigned according to Table 6.2. The virtual wall has a damping of $60 \frac{N \cdot s}{m}$, and a stiffness of $6000 \frac{N}{M}$. Fig. 6.4 depicts the experimental results for the linear case where $k_f = 1$.

Next the proposed controller was tested with the monotonic nonlinear force mapping $k_f^{-1}(f) = f(1 - 0.2 \tanh((\frac{f}{8})^2))$ depicted in Fig. 6.5. The argument f was $H_{fh1}f_h^1 + H_{fh2}f_h^2 - H_{zt}x_e$. This choice of $k_f^{-1}(f)$ satisfies the conditions provided in [7] for enhanced stiffness discrimination. In either free motion or contact with the wall at $x_{wall} = 0.03$, the ability to track the other user and the environment position is evident in both Figs. 6.4 and 6.5. The force tracking objective (4.19) has also been attained as can be seen in the last diagram of each figure. The virtual tool mass for the admittance-type was set to 0.35 kg.

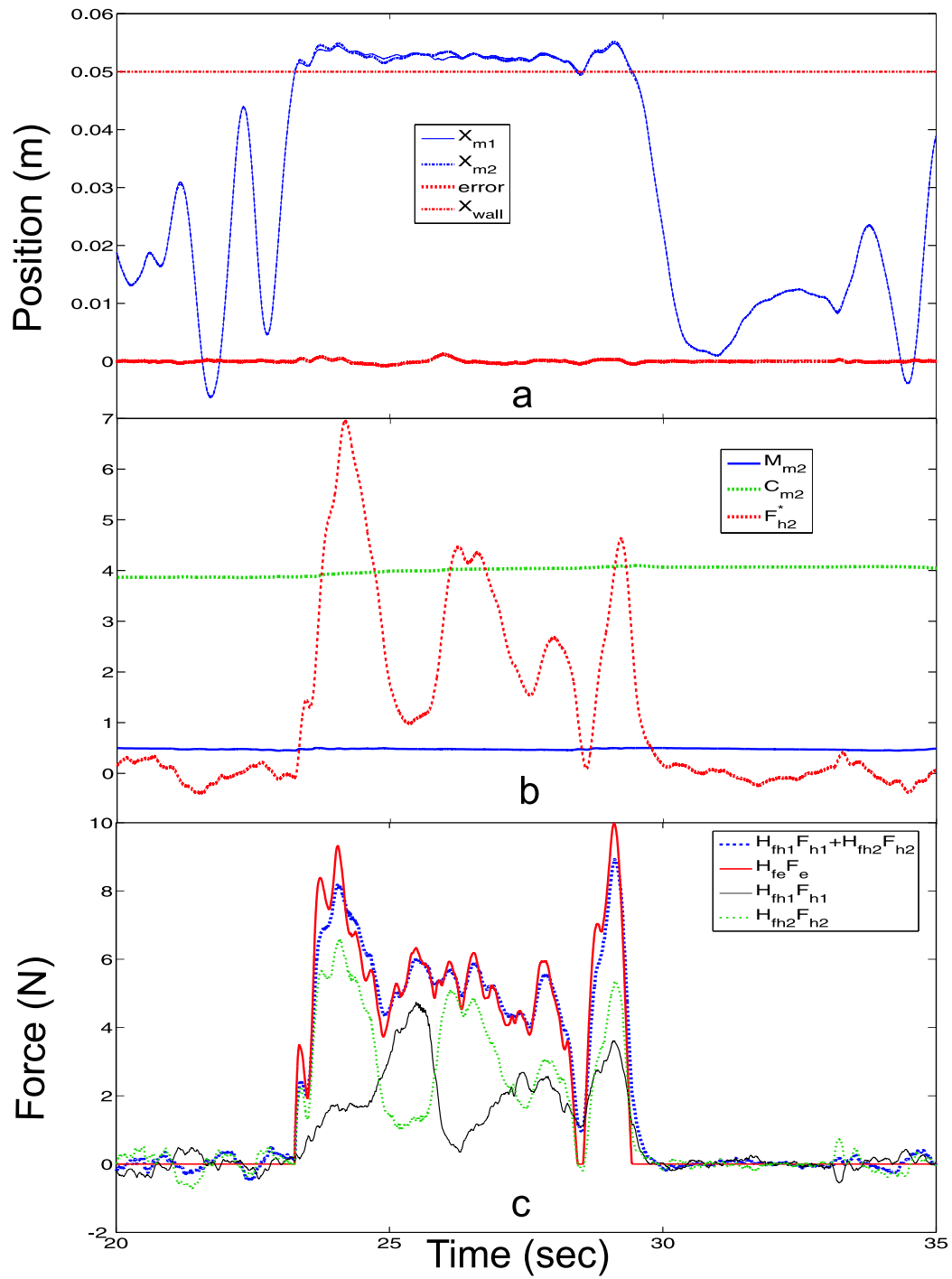


Figure 6.2: Impedance-type with linear filters (a) Positions. (b) Estimated parameters. (c) $H_{fh1}F_h^1 + H_{fh2}F_h^2, H_{fe}F_e, H_{fh1}F_h^1$, and $H_{fh2}F_h^2$.

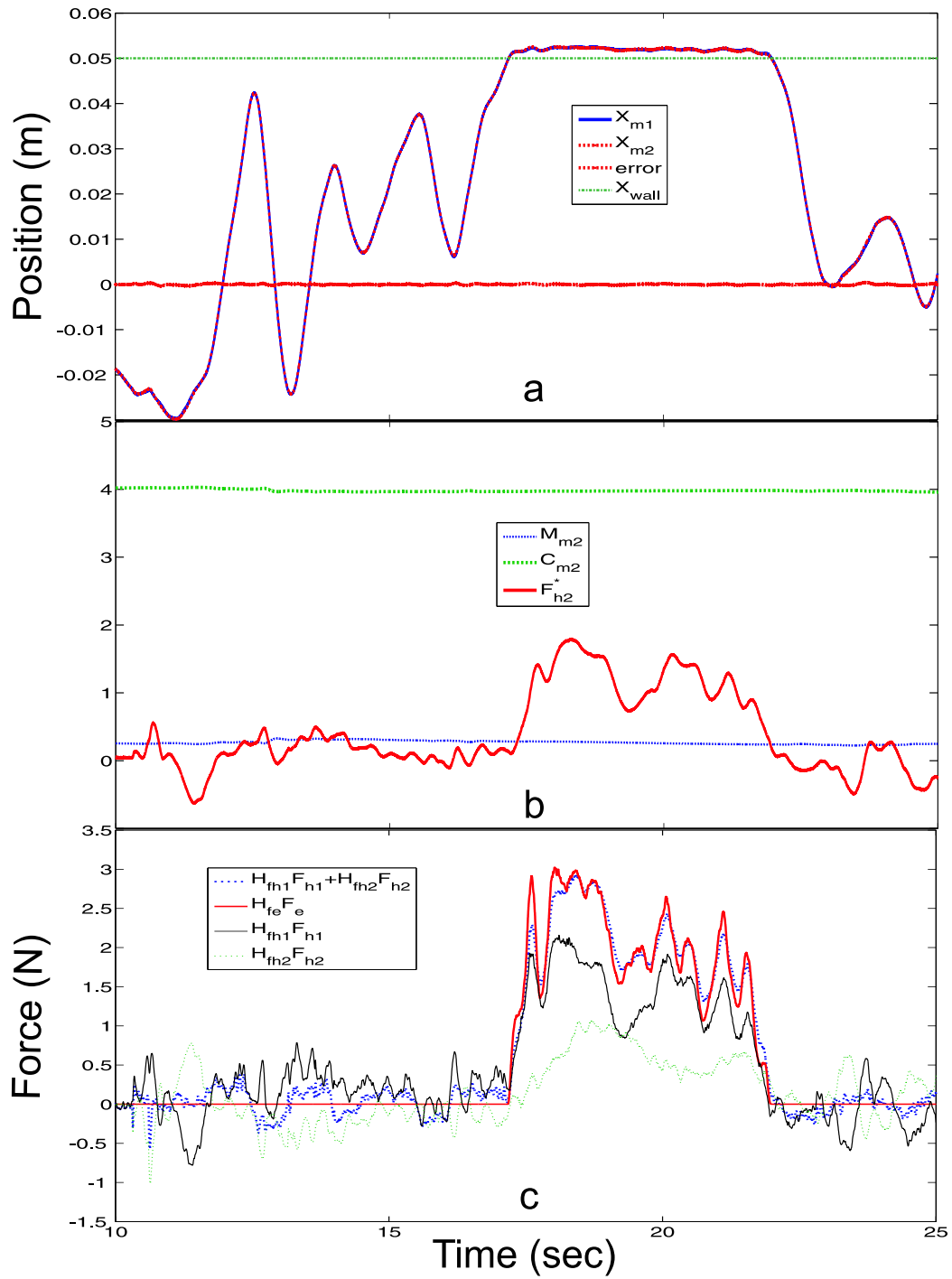


Figure 6.3: Impedance-type with a nonlinear mapping as k_f (a) Positions. (b) Estimated Parameters. (c) $H_{fh1}F_h^1 + H_{fh2}F_h^2, H_{fe}F_e, H_{fh1}F_h^1$, and $H_{fh2}F_h^2$.

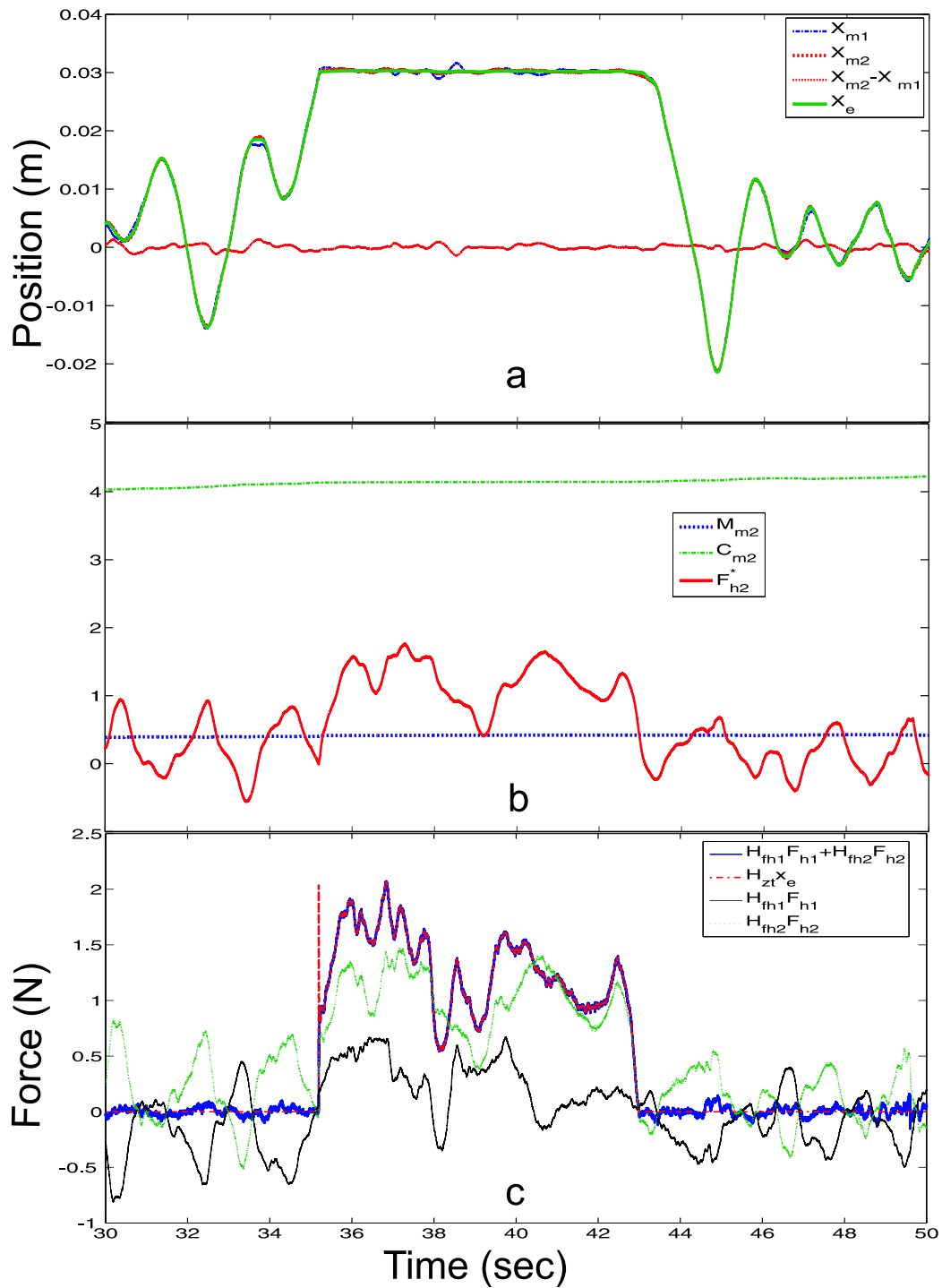


Figure 6.4: Admittance-type with linear filters (a)Positions. (b)Estimated parameters. (c) $H_{fh1}F_h^1 + H_{fh2}F_h^2, H_{zt}x_e, H_{fh1}F_h^1$, and $H_{fh2}F_h^2$.

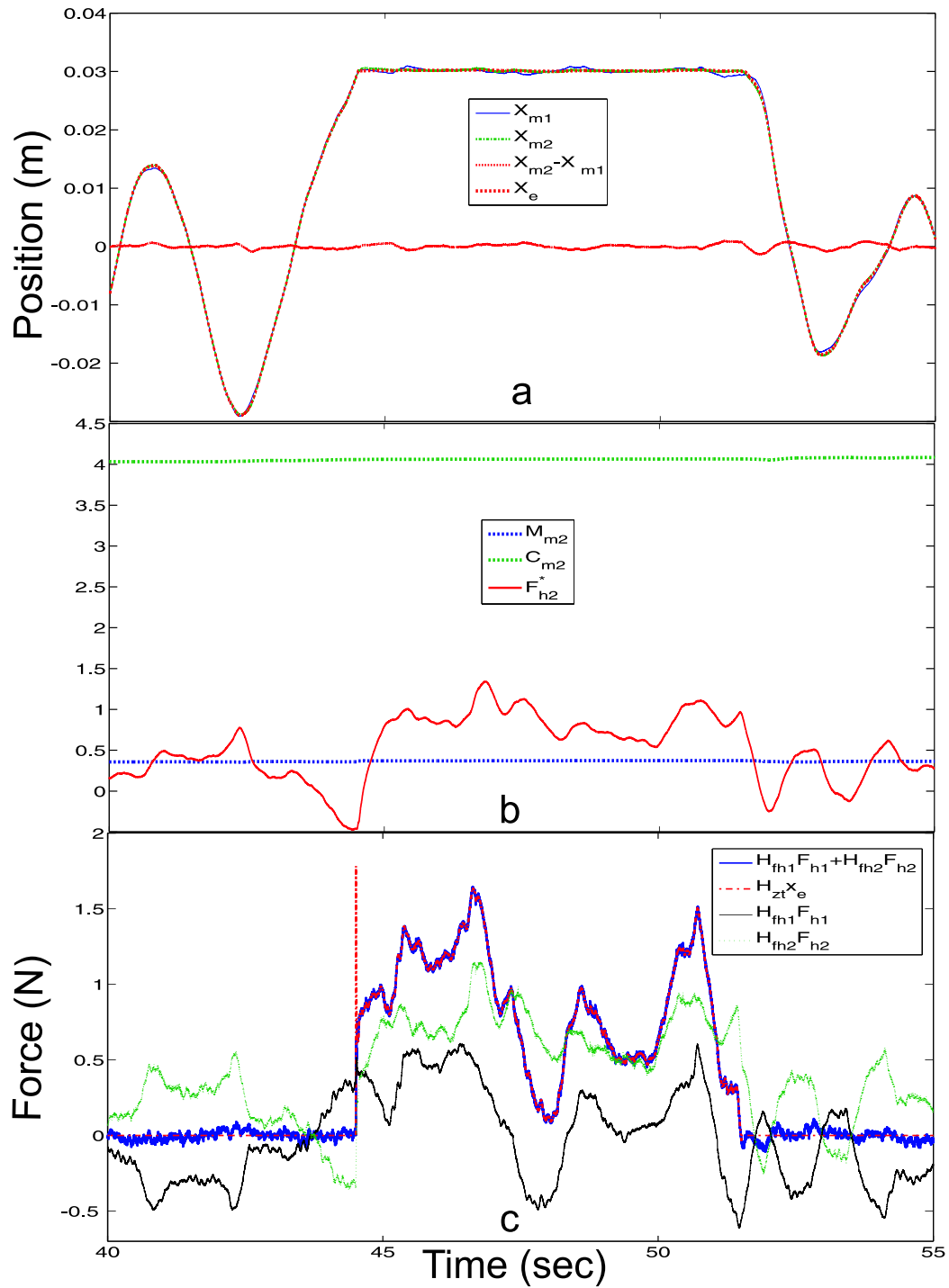


Figure 6.5: Admittance-type with a nonlinear mapping as k_f (a) Positions. (b) Estimated parameters. (c) $H_{fh1}F_h^1 + H_{fh2}F_h^2, H_{zt}x_e, H_{fh1}F_h^1,$ and $H_{fh2}F_h^2$.

Chapter 7

Conclusions and Future Work

This thesis was concerned about control design and psychophysics evaluation of a haptic-enabled collaborative virtual environments for skills training. Using virtual reality for skills training purposes are an emerging field of research. In these algorithms, after the workspace is modeled in a virtual reality simulator, the subjects can learn and practice the real world tasks. The use of haptics (providing kinesthetic and force feedback from virtual tasks) in conjunction with virtual reality can improve the realism of the human operator experience when dealing with the virtual task and is used in a wide range of applications. The collaborative haptic training using virtual reality simulators is an example of these applications. This framework can potentially improve the conventional teaching schemes by linking the trainer and trainee and the virtual environment. A similar attempt in real world training session will lead to awkward tool manipulation and will degrade the ergonomics of learning. However, in the method known as collaborative training or haptic-guidance the connection is made through the control system and the instructor and the student will be working with two separate haptic devices and

in the mean time will feel each other.

The contributions of this thesis can be summarized as:

- A set of psychophysical experiments were designed to explore the use of collaborative haptic training. The subjects were divided to two groups: the ones that received training and the ones who did not. The results of these experiments confirmed the effectiveness of collaborative training in improving users temporal response in the experimental scenario. Based on the results the trained group also showed a better performance in trajectory tracking with less overall error.
- Active participation of the trainee was found to be an important factor in the effectiveness of human-haptic training. In addition, human-haptic guidance was shown to be most effective in improving trajectory tracking accuracy in the experiment where the visual feedback was most defective.
- The results of the human factor studies motivated the design of a framework for collaborative haptic training using adaptive control. In this framework, two users were linked through a virtual tool using which they could practice different tasks cooperatively in a virtual reality model. The design allowed for various linear time invariant filters and nonlinear mappings for impedance and admittance environment types.
- Through a Lyapunov analysis, it was shown that the proposed controller can achieve the generalized position tracking and impedance shaping objectives.
- To ensure closed-loop stability of the system in the presence of the uncertainties in the user and environment dynamics, a robust control analysis was

performed. Robust stability regions were investigated for different mapping parameters using the Nyquist envelop of interval plants and an off-axis circle criterion..

In future, we hope to develop application specific training platforms and use more general force and position mappings in the control structure [53] to improve the performance of the system at different stages of the task such as contact and stiffness perception. Other human factor studies can be designed to achieve different helpful force and position mappings. The ability of the users to recall their trainings after a longer time period can also be investigated through psychophysics studies, thus, enabling the evaluation of the training method in long term skills training.

Bibliography

- [1] E. L. Faulring, J. E. Colgate, and M. A. Peshkin, "High performance cobotics," in *International Conference on Rehabilitation Robotics*, pp. 143–148, 2005.
- [2] U. Kuhnappel, H. K. Cakmak, B. Chantier, H. Maass, G. Strauss, C. Trantakis, E. Novatius, J. Meixensberger, K. Lehmann, H. J. Buhr, M. Lawo, and G. Bretthauer, "Hapticio: haptic interface-systems for virtual-reality training in minimally-invasive surgery," in *the Internationale Statustagung Virtuelle und Erweiterte Realitt Leipzig*, pp. 19–20, 2004.
- [3] B. J. M. M. G. M. R. W. Webster, D. I. Zimmerman, "A prototype haptic suturing simulator," *Medicine Meets Virtual Reality, IOS Press*.
- [4] R. J. Adams, M. R. Moreyra, and B. Hannaford, "Stability and performance of haptic displays: Theory and experiments," in *Proc. ASME Int. Mech. Eng. Congr. Exh., Anaheim, CA*, p. 227234, 1998.
- [5] M. Ueberle and M. Buss, "Control of kinesthetic haptic interfaces," in *IEEE/RSJ Int. Conf. on Intellig. Rob. and Syst., Workshop on Touch and Haptics*, 2004.

- [6] L. B. Rosenberg, "Virtual fixtures: Perceptual tools for telerobotic manipulation," in *IEEE Virtual Reality Int. Symp. (VRAIS93)*, pp. 76–82, 1993.
- [7] P. Malysz and S. Sirouspour, "Generalized force/position mappings in bilateral teleoperation with application to enhanced stiffness discrimination (submitted)," *IEEE Transaction on Robotics*.
- [8] P. Malysz and S. Sirouspour, "Enhanced bilateral teleoperation using general force/position mapping," in *IEEE International Conference Robotics and Automation*, pp. 4307–12, 2007.
- [9] W. H. Zhu and S. E. Salcudean, "Stability guaranteed teleoperation: an adaptive motion/force control approach," *IEEE Transactions on Automatic Control*, vol. 45, pp. 1951–1969, Nov. 2000.
- [10] P. Brown, D. Jones, and S. K. Singh, "The exoskeleton glove for control of paralyzed hands," in *IEEE International Conference on Robotics and Automation*, pp. 642–647, 1993.
- [11] S. Sirouspour and A. Shahdi, "A six degree-of-freedom magnetically levitated variable compliance fine motion wrist: design, modelling, and control," *IEEE Transactions on Robotics and Automation*, vol. 7, no. 3, pp. 320–332, 1991.
- [12] Z. Xu and D. Taylor, "Using motion platform as a haptic display for virtual inertia simulation," in *the proc. of Seventh International Conference on Information Visualization*, pp. 498–504, 2003.

- [13] E. L. Faulring, J. E. Colgate, and M. A. Peshkin, "A high performance 6-dof haptic cobot," in *IEEE International Conference on Robotics and Automation, New Orleans*, pp. 1980–1985, 2004.
- [14] R. Q. van der Linde and P. Lammertse, "Hapticmaster a generic force controlled robot for human interaction," *Industrial Robot: An International Journal*, vol. 30, no. 6, pp. 515–524, 2003.
- [15] D. A. Lawrence, "Stability and transparency in bilateral teleoperation," *IEEE Trans. Robot. Automat.*, vol. 9, pp. 624–637, Oct. 1993.
- [16] R. J. Adams and B. Hannaford, "A two-port framework for the design of unconditionally stable haptic interfaces," in *International Conference on Intelligent Robots and Systems (IROS)*, 1998.
- [17] J. E. Colgate and J. M. Brown, "Factors affecting the z-width of a haptic display," in *IEEE Conference on Robotics and Automation*, pp. 3205–3210, 1994.
- [18] B. Gillespie and M. Cutkosky, "Effects of position quantization and sampling rate on virtual-wall passivity," *IEEE Transactions on Robotics*, vol. 21, pp. 952–964, Oct 2005.
- [19] N. Diolaiti, G. Niemeyer, F. Barbagli, and J. K. Salisbury, "A criterion for the passivity of haptic devices," in *2005 IEEE International Conference on Robotics and Automation*, 2005.
- [20] R. J. Adams and B. Hannaford, "Control law design for haptic interfaces to virtual reality," *IEEE Transactions on Control Systems Technology*, vol. 10, pp. 3–13, Jan 2002.

- [21] J. E. Colgate and G. G. Schenkel, "Passivity of a class of sampled-data systems: Application to haptic interfaces," *Journal of Robotic Systems.*, vol. 14, pp. 37–47, Jan 1997.
- [22] N. Diolaiti, G. Niemeyer, and N. A. Tanner, "Wave haptics: Building stiff controllers from the natural motor dynamics," *The International Journal of Robotics Research*, vol. 26, pp. 5–21, Jan 2007.
- [23] A. Gosline and V. Hayward, "Time-domain passivity control of haptic interfaces with tunable damping hardware," in *the Proc. of Second Joint EuroHaptics Conference and Symposium on Haptic Interfaces for Virtual Environment and Teleoperator System*, pp. 164–179, 2007.
- [24] A. Abdossalami and S. Sirouspour, "Adaptive control for transparent haptic interaction with virtual environments," in *to appear in IEEE Transactions on Haptics*, 2009.
- [25] S. Nudehi, R. Mukherjee, and M. Ghodoussi, "A shared approach to haptic interface design for minimally invasive telesurgical training," *IEEE Transactions on Control Systems Technology*, vol. 13, no. 4, pp. 588–592, 2005.
- [26] J. Helton and . Merino, *Classical control using H_∞ , methods: theory, optimization and design*. SIAM, 1998.
- [27] S. Sirouspour, "Modelling and control of cooperative teleoperation systems," *IEEE Transaction on Robotics*, vol. 21, pp. 1220–1225, Dec. 2005.

- [28] S. Sirouspour and P. Setoodeh, "Adaptive nonlinear teleoperation control in multi-master/multi-slave environments," in *IEEE Conference Control Application*, pp. 1263–1268, Aug. 2005.
- [29] S. Niakosari and S. Sirouspour, "Improving transparency in network-based haptics," (to appear in) *World HAPTICS Conference*, March 2009.
- [30] M. Fotoohi, S. Sirouspour., and D. Capson, "Multi-rate control architectures for dextrous haptic rendering in cooperative virtual environments," in *IEEE Conference on Decision and Control*, pp. 4478–4483, 2005.
- [31] B. Khademian and K. Hashtrudi-Zaad, "Performance issues in collaborative haptic training," in *IEEE International Conference on Robotics and Automation*, pp. 3257 – 3262, 2007.
- [32] B. Khademian and K. Hashtrudi-Zaad, "A robust multilateral shared controller for dual-user teleoperation systems," in *Canadian Conference on Electrical and Computer Engineering CCECE*, pp. 001871–001876, 2008.
- [33] C. Gunn, M. Hutchins, M. Adcock, and R. Hawkins, "Surgical training using haptics over long internet distances," in *Proceedings of Medicine Meets Virtual Reality 12*, 2004.
- [34] C. Gunn, M. Hutchins, D. Stevenson, M. Adcock, and P. Youngblood, "Using collaborative haptics in remote surgical training," in *Proceedings of WorldHaptics*, 2005.

- [35] J. Kim, H. Kim, M. Muniyandi, M. Srinivasan, J. Jordan, J. Mortensen, M. Oliveira, and M. Slater, "Transatlantic touch: a study of haptic collaboration over long distance," *Presence: Teleoper Virtual Environ*, vol. 13, no. 3, pp. 328–337, 2004.
- [36] K. Henmi and T. Yoshikawa, "Virtual lesson and its application to virtual calligraphy system," in *IEEE Conf. on Robotics and Automation*, pp. 1275–1280, 1998.
- [37] Y. Yokokohji, R. Hollis, T. Kanade, K. Henmi, , and T. Yoshikawa, "Toward machine mediated training of motor skill," in *IEEE International Workshop on Robot and Human Communication*, pp. 32–37, 1996.
- [38] C. Carignan and P. Olsson, "Cooperative control of virtual objects over the internet using force-reflecting master arms," in *in Proc. IEEE Int. Conf. on Robotics and Automation*, pp. 1221–1226, 2004.
- [39] D. J. Reinkensmeyer and J. L. Patton, "Can robots help the learning of skilled actions," *Exerc. Sport Sci. Rev.*, vol. 37, no. 1, pp. 43–51, 2009.
- [40] D. Feygin, M. Keehner, and F. Tendick, "Haptic guidance: experimental evaluation of a haptic training method for a perceptual motor skill," in *10th Int. Symp. Haptic Interfaces for Virtual Environment and Teleoperator Systems, Orlando*, pp. 40–47, 2002.
- [41] J. Liu, S. Cramer, and D. Reinkensmeyer, "Learning to perform a new movement with robotic assistance: comparison of haptic guidance and visual demonstration," *Journal of NeuroEngineering and Rehabilitation*, vol. 3,

pp. 1743–0003, Aug. 2006.

- [42] D. Morris, H. Tan, F. Barbagli, T. Chang, and K. Salisbury, “Haptic feedback enhances force skill learning,” in *Second joint EuroHaptics Conference and Symposium on Haptic Interfaces for Virtual Environment and Teleoperator Systems*, pp. 21–26, 2007.
- [43] L. B. Rosenberg, “Virtual fixtures: perceptual tools for telerobotic manipulation,” in *IEEE Virtual Reality International Symposium (VRAIS)*, pp. 76–82, 2007.
- [44] L. Sciavicco and B. Siciliano, *Modeling and control of robot manipulators*. Springer-Verlag, second ed., 2000.
- [45] M. A. Hitz and E. Kaltofen, “The kharitonov theorem and its applications in symbolic mathematical computation,” in *Workshop on Symbolic-Numeric Algebra for Polynomials (SNAP96)*, July 1996.
- [46] B. R. Barmish, “A generalization of kharitonov’s four polynomials concept for robust stability problems with linearly dependent coefficient perturbations,” *IEEE Transactions on Automatic Control*, vol. 34, pp. 157–165, 1989.
- [47] N. Tan and D. Atherton, “Frequency response of uncertain systems a 2q-convex parpolygonal approach,” in *IEEE Control Theory Applications*, vol. 147, pp. 547–555, Sept. 2000.
- [48] G. Zames, “On the input-output stability of time-varying nonlinear feedback systems part i: conditions derived using concepts of loop gain, conicity, and positivity,” *IEEE Transactions on Automatic Control*, vol. AC-11, no. 2, pp. 228–238, 1966.

- [49] Y.-S. Cho and K. S. Narendra, "An off-axis circle criteria for the stability of feedback systems with monotonic nonlinearity," *IEEE Transactions on Automatic Control*, vol. 13, pp. 413–416, 1968.
- [50] C. V. Hollot and T. R., "On the nyquist envelope of an interval plant family," *IEEE Transactions on Automatic Control*, vol. 39, pp. 391–396, Feb. 1994.
- [51] S. P. Bhattacharyya, H. Chapellat, and L. H. Keel, *Robust control: the parametric approach*. Prentice Hall, 1995.
- [52] A. Barlett, C. V. Hollot, and H. Lin, "Root location of an entire polytope of polynomials: it suffices to check the edges," *Math. Control, Signals. Syst.*, no. 1, pp. 61–71, 1988.
- [53] S. Moghimi, S. Sirouspour, and P. Malysz, "Haptic-enabled collaborative training with generalized force and position mappings," in *symposium on Haptic interfaces for virtual environment and teleoperator systems*, pp. 287–294, 2008.